

PL-TR--91-1036

AD-A243 551

PL-TR--
91-1636



2200 790

2

**FREQUENCY STIRRING: AN ALTERNATE APPROACH
TO MECHANICAL MODE-STIRRING FOR THE
CONDUCT OF ELECTROMAGNETIC SUSCEPTIBILITY
TESTING**

Thomas A. Loughry

November 1991

Final Report

DTIC
ELECTE
NOV 18 1991
S B D

APPROVED FOR PUBLIC RELEASE; DISTRIBUTION UNLIMITED.



PHILLIPS LABORATORY
Directorate of Advanced Weapons and Survivability
AIR FORCE SYSTEMS COMMAND
KIRTLAND AIR FORCE BASE, NM 87117-6008

91-15803



20000 901 023

PL-TR--91-1036

This final report was prepared by the Phillips Laboratory, Kirtland Air Force Base, New Mexico, under Job Order ILIR9012. The Laboratory Project Officer-in-Charge was Capt Thomas A. Loughry (PL/WSMM).

When Government drawings, specifications, or other data are used for any purpose other than in connection with a definitely Government-related procurement, the United States Government incurs no responsibility or any obligation whatsoever. The fact that the Government may have formulated or in any way supplied the said drawings, specifications, or other data, is not to be regarded by implication, or otherwise in any manner construed, as licensing the holder, or any other person or corporation; or as conveying any rights or permission to manufacture, use, or sell any patented invention that may in any way be related thereto.

This report has been authored by an employee of the United States Government. Accordingly, the United States Government retains a nonexclusive royalty-free license to publish or reproduce the material contained herein, or allow others to do so, for the United States Government purposes.

This report has been reviewed by the Public Affairs Office and is releasable to the National Technical Information Service (NTIS). At NTIS, it will be available to the general public, including foreign nationals.

If your address has changed, please notify PL/WSMM, Kirtland AFB, NM 87117-6008, to help us maintain a current mailing list.

This report has been reviewed and is approved for publication.

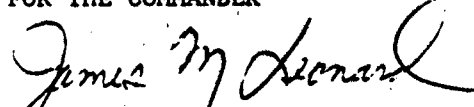


THOMAS A. LOUGHRY, Capt, USAF
Project Officer



WAYNE J. ANDERSON, Lt Col, USAF
Chief, Microwave Effects Branch

FOR THE COMMANDER



JAMES M. LEONARD, Lt Col, USAF
Chief, Directed Energy Effects
Division

DO NOT RETURN COPIES OF THIS REPORT UNLESS CONTRACTUAL OBLIGATIONS OR NOTICE ON A SPECIFIC DOCUMENT REQUIRES THAT IT BE RETURNED.

REPORT DOCUMENTATION PAGE

Form Approved
OMB No. 0704-0188

Public reporting burden for this collection of information is estimated to average 1 hour per response, including the time for reviewing instructions, searching existing data sources, gathering and maintaining the data needed, and completing and reviewing the collection of information. Send comments regarding this burden estimate or any other aspect of this collection of information, including suggestions for reducing this burden, to Washington Headquarters Services, Directorate for Information Operations and Reports, 1215 Jefferson Davis Highway, Suite 1204, Arlington, VA 22202-4302, and to the Office of Management and Budget, Paperwork Reduction Project (0704-0188), Washington, DC 20503.

| | | | | | |
|--|--|--|--|--|--|
| 1. AGENCY USE ONLY (Leave blank) | | 2. REPORT DATE November 1991 | | 3. REPORT TYPE AND DATES COVERED Final Apr 90 - Apr 91 | |
| 4. TITLE AND SUBTITLE FREQUENCY STIRRING: AN ALTERNATE APPROACH TO MECHANICAL MODE-STIRRING FOR THE CONDUCT OF ELECTROMAGNETIC SUSCEPTIBILITY TESTING | | | | 5. FUNDING NUMBERS PE: 61101F PR: ILIR TA: 90 WU: 12 | |
| 6. AUTHOR(S) Thomas A. Loughry | | | | | |
| 7. PERFORMING ORGANIZATION NAME(S) AND ADDRESS(ES) Phillips Laboratory Kirtland AFB, NM 87117-6008 | | | | 8. PERFORMING ORGANIZATION REPORT NUMBER PL-TR-91-1036 | |
| 9. SPONSORING/MONITORING AGENCY NAME(S) AND ADDRESS(ES) | | | | 10. SPONSORING/MONITORING AGENCY REPORT NUMBER | |
| 11. SUPPLEMENTARY NOTES | | | | | |
| 12a. DISTRIBUTION/AVAILABILITY STATEMENT Approved for public release; distribution is unlimited. | | | | 12b. DISTRIBUTION CODE | |
| 13. ABSTRACT (Maximum 200 words) This report summarizes the results of an experiment designed to determine the effectiveness of using frequency stirring to provide field homogeneity in a reverberation chamber. Frequency stirring is accomplished by up-converting band limited white Gaussian noise to microwave frequencies and thus exploits both the high mode densities achievable in a narrow bandwidth at microwave frequencies and the pseudo-statistical nature of the reverberation chamber's eigenmodes. The ultimate goal is to replace the mechanical stirring device currently used in reverberating chambers with an equivalent electronic eigenmode stirrer. In addition, an expression for the net Q of a reverberation chamber is developed which includes the effects of antenna loading; methods for predicting the homogeneity of the resulting fields in the chamber after application of the frequency stir technique are proposed; and a theoretical basis for interpreting fringe power density levels, cross sections, and shielding effectiveness measurements is also given. | | | | | |
| 14. SUBJECT TERMS Reverberating chamber, mode-stir chamber, electromagnetic compatibility and vulnerability measurements, frequency stirring, quality factor, Q, microwave susceptibility/vulnerability testing, cross section, shielding effectiveness | | | | 15. NUMBER OF PAGES 56 | |
| | | | | 16. PRICE CODE | |
| 17. SECURITY CLASSIFICATION OF REPORT Unclassified | | 18. SECURITY CLASSIFICATION OF THIS PAGE Unclassified | | 19. SECURITY CLASSIFICATION OF ABSTRACT Unclassified | |
| | | | | 20. LIMITATION OF ABSTRACT III | |

CONTENTS

| <u>Section</u> | <u>Page</u> |
|--|-------------|
| INTRODUCTION | 1 |
| THEORETICAL DEVELOPMENT | 4 |
| B-DOT PROBES | 4 |
| RECTANGULAR CAVITIES | 4 |
| FREQUENCY STIRRING | 22 |
| PREFERRED METHOD | 22 |
| FIELD HOMOGENEITY PREDICTIONS | 25 |
| COUPLING CROSS SECTIONS | 29 |
| SHIELDING EFFECTIVENESS | 33 |
| UPSET THRESHOLD TESTING | 33 |
| TEST CONFIGURATIONS | 35 |
| FIELD UNIFORMITY SWEPT MEASUREMENTS (NT Enclosure) | 35 |
| FIELD UNIFORMITY SWEPT MEASUREMENTS (GIFT Box) | 37 |
| THE Q MEASUREMENTS (NT and GIFT Box) | 37 |
| TEST PROCEDURES | 40 |
| FIELD UNIFORMITY TESTS | 40 |
| THE Q MEASUREMENTS | 42 |
| RESULTS | 44 |
| SWEPT MEASUREMENTS | 44 |
| Q MEASUREMENTS | 48 |
| CONCLUSIONS | 50 |
| REFERENCES | 51 |



| | |
|--------------------|-------------------------------------|
| Accession For | |
| NTIS GRA&I | <input checked="" type="checkbox"/> |
| DTIC TAB | <input type="checkbox"/> |
| Unannounced | <input type="checkbox"/> |
| Justification | |
| By | |
| Distribution/ | |
| Availability Codes | |
| Dist | Avail and/or Special |
| A-1 | |

FIGURES

| <u>Figure</u> | | <u>Page</u> |
|---------------|--|-------------|
| 1. | The NT enclosure. | 2 |
| 2. | The GIFT box enclosure. | 2 |
| 3. | Mode density as a function of the agility bandwidth and center frequency for a 1-m ³ cavity. | 6 |
| 4. | Cavity orientation used to derive fields (from Ref. 4). | 7 |
| 5. | Three different directions of propagation. | 10 |
| 6. | Surface of constant k_r . | 12 |
| 7. | Effect of probes and antenna on the net Q. | 19 |
| 8. | Theoretical and Measured Q for the NIST chamber. | 21 |
| 9. | Frequency stir spectrum. | 24 |
| 10. | Output of the up-converters for a center frequency of 1.5 GHz and all four agility bandwidths. | 24 |
| 11. | Measured cross section when the bandwidth of resonance is smaller than the bandwidth of the gating function. | 32 |
| 12. | Measured cross section when the bandwidth of resonance is greater than the bandwidth of the gating function. | 32 |
| 13. | Experimental setup for swept tests on the NT enclosure. | 36 |
| 14. | The NT enclosure: view of horn and probes. | 36 |
| 15. | Experimental test setup for swept tests on the GIFT box enclosure. | 38 |
| 16. | The GIFT box enclosure: view of horn and probes. | 39 |
| 17. | Test configuration used to measure Q of the NT enclosure. | 39 |
| 18. | Measured power ratios of probes C and D for the NT enclosure with an agility bandwidth of 0, 10, 50 and 100 MHz. | 44 |

FIGURES (Continued)

| <u>Figure</u> | | <u>Page</u> |
|---------------|---|-------------|
| 19. | Goodness of fit test, NT enclosure, 10 MHz agility bandwidth, 1 to 2 GHz. | 47 |
| 20. | Measured Q for both enclosures. | 49 |

TABLES

| <u>Table</u> | | <u>Page</u> |
|--------------|---|-------------|
| 1. | Standard deviation of field ratios for different values of N. | 28 |
| 2. | Homogeneity measurements for the NT enclosure. | 45 |
| 3. | Homogeneity measurements for the GIFT box. | 46 |

INTRODUCTION

There has been an increasing interest in the use of mode tuned or stirred reverberation chambers for conducting electromagnetic coupling and upset experiments. Mode-stir chambers consist of a high quality factor (Q) metallic reverberation chamber in which a stirring device such as a metallic paddle wheel is used to incrementally or continuously alter the boundary conditions within the chamber. The goal is to achieve an isotropic homogeneous field everywhere in the volume of the cavity except near the walls. Field homogeneity is achieved in this manner by exploiting the pseudo-statistical nature of each of the eigenfunction's contribution to the field level at a given point well within the chamber volume. Extensive work has been done by the National Institute of Standards and Technology (NIST) (previously the National Bureau of Standards) and the Naval Surface Weapons Center to both optimize chamber design and characterize chamber fields. The NIST has achieved field uniformities of $< \pm 3$ dB above 1 GHz and $< \pm 2$ dB above 2 GHz in a 2.74 x 3.05 x 4.75 m welded steel enclosure using the paddle wheel technique [Ref. 1].

Reverberation chamber testing offers several advantages over anechoic or plane wave illumination testing. For example, E-field levels in the thousands of volts per meter can be achieved using modestly low power sources such as 200 W TWT amplifiers. Coupling cross sections can be measured independent of the angle of incidence (this is particularly beneficial when testing subsystems that would normally exist inside an equipment bay or cavity). On the other hand, dependence on mechanical mode stirring can complicate data acquisition and interpretation as well as require long periods of time (as much as 10 hours per test) to acquire a complete data set. These complications are primarily due to the requirement that data be measured for many different positions of the paddle wheel for each frequency and power level because field uniformity inside the volume of the chamber can only be obtained by averaging the fields influenced by each position of the tuner over many positions. Hence, real time field uniformity can only exist on time scales of the same order as the paddle wheel rotation rate.

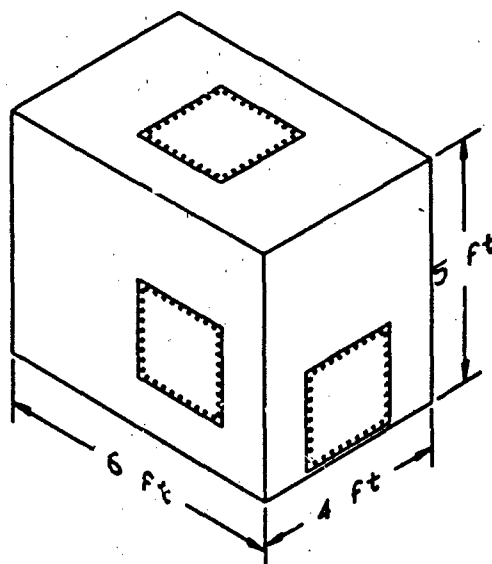


Figure 1. The NT Enclosure.

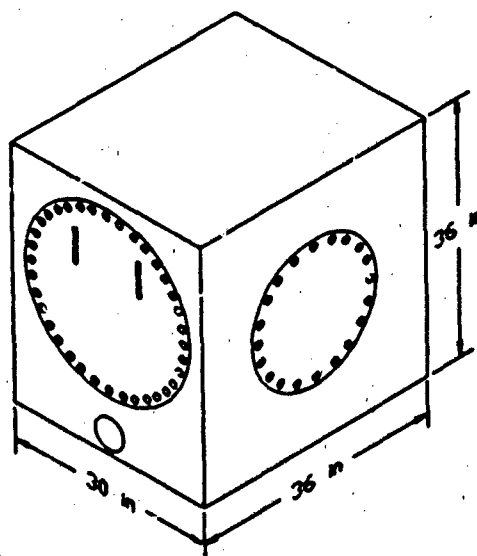


Figure 2. The GIFT box enclosure.

It was the purpose of this experiment to investigate the use of electronic mode stirring in a reverberation chamber to perform both coupling and upset testing. While the conventional method of mode stirring holds the frequency constant and varies the cavity's boundary conditions in order to obtain a sufficiently large sample of eigenfunction contributions to the field levels at a given point in the chamber, the method described here does not vary the

boundary conditions, but instead averages the eigenfunction's contributions over a narrow band of frequency. Expected advantages of this technique over the more conventional method included shorter test times (from hours to less than 5 minutes), simplified data acquisition and control, and more interpretable results. Because of their availability and in order to determine the effect chamber size has on the technique, two separate reverberation chambers were chosen, one relatively small and one relatively large (Figures 1 and 2). The larger enclosure is referred to as the NT enclosure because it was borrowed from the Nuclear Technology (NT) Directorate here at the Weapons Laboratory (now the Phillips Laboratory), while the other is referred to as the GIFT box (an acronym from a previous test).

THEORETICAL DEVELOPMENT

B-DOT PROBES

There are several different sensors available for measuring electric and magnetic fields. B-dot probes were chosen for this experiment because of their availability, small size, and broad bandwidth. The voltage output of the B-dot probe is directly proportional to both the probe's effective area A_e , and the time rate of change of the B field dotted into the normal vector to the plane of the probe's loop:

$$v(t) = A_e \cdot \frac{dB}{dt} \cdot \hat{n} \quad (1)$$

Since only continuous wave signals are used in this experiment, it is more useful to consider the Fourier transform of the above expression:

$$G(j\omega) = \frac{V(j\omega)}{\hat{n} \cdot B(j\omega)} = jA_e \omega \quad (2)$$

where $G(j\omega)$ is the transfer function that relates the voltage output to the amplitude and phase of the B field. At a fixed frequency, ω , the power density, P_d , due to the component of the B field normal to the probe loop, B_n , can be related to the probe's power output, P_m into a 50 Ω instrument as follows:

$$\begin{aligned} \text{Since } P_d &= \frac{1}{2} \frac{c B_n^2}{\mu_0} \\ P_m(\omega) &= \frac{1}{2} \frac{1}{50} |G(j\omega)|^2 |B_n(j\omega)|^2 = \frac{\mu_0 A_e^2}{50c} \omega^2 P_d \end{aligned} \quad (3)$$

where c is the speed of light and μ_0 is the permeability of free space (the medium is assumed to be a vacuum). The expression for the power density, P_d , above was found by multiplying the energy density of a plane wave by the speed of light.

RECTANGULAR CAVITIES

Electromagnetic theory as applied to conductive rectangular cavities can be found in many standard electromagnetic texts and reports. For convenience, several of the more important results are repeated here.

The frequencies at which eigenmodes can exist in a rectangular cavity of dimensions a , b , and d are [Ref. 2, pp 345]:

$$f_{mnl} = \frac{c}{2\pi\sqrt{\mu_r\epsilon_r}} \sqrt{\left(\frac{m\pi}{a}\right)^2 + \left(\frac{n\pi}{b}\right)^2 + \left(\frac{l\pi}{d}\right)^2} \quad (4)$$

where

- m, n, l - Any set of integers ≥ 0 except $(0,0,0)$.
- c - Speed of light.
- μ_r, ϵ_r - Relative permeability and permittivity of the medium filling the cavity.

Of more interest, however, is the total number of eigenmodes that can exist in a small interval of frequency with a center frequency of f . This quantity is referred to as the specific mode density. Blackbody mode density calculation results are directly analogous to this problem and express the mode density as [Ref. 3]:

$$dN = \frac{8\pi abd}{c^3} f^2 df \quad (5)$$

Mode density is important because it determines the effective sample size of the pseudo-random eigenfunction amplitudes at the point of interest. The larger the effective sample size, the better the statistical randomness of the eigenfunction amplitudes at a given point and the better the field homogeneity. The theoretical mode density for a 1-m³ cavity with several different frequency agile source bandwidths is shown in Figure 3.

Another important parameter is the quality factor Q :

$$Q = 2\pi \frac{\text{Energy Stored}}{\text{Power Lost / Hertz}} = \omega_0 \frac{\text{Energy Stored}}{P_r} \quad (6)$$

where P_r is the net power being transmitted into the enclosure and ω_0 is the radian frequency of the exciting source.

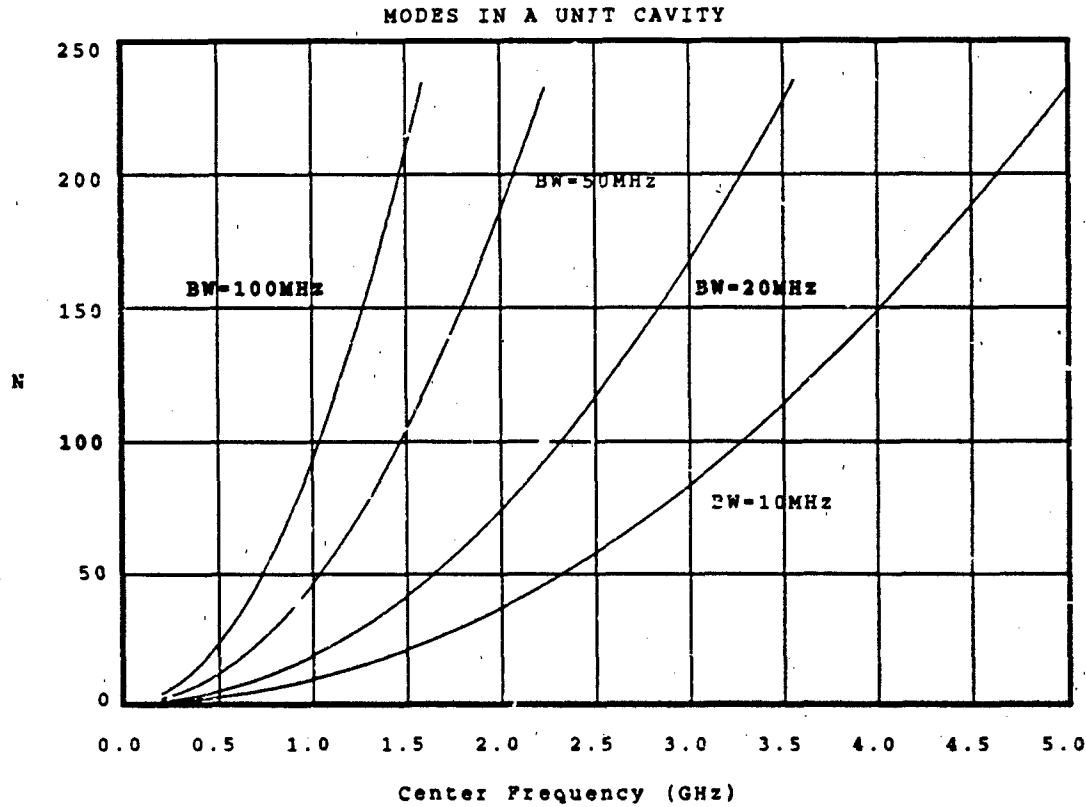


Figure 3. Mode density as a function of the agility bandwidth and center frequency for a 1-m³ cavity.

Composite Q of a Rectangular Cavity

The expression given above for the Q of a cavity is singular in frequency. In other words, the equation assumes that P_T is a monochromatic source with frequency ω_0 . If instead the spectrum of P_T is spread across a narrow band of frequency (as is the case for this experiment), it is convenient to derive an expression for a composite Q that presents the net effect of having many eigenmodes stimulated simultaneously. More specifically:

$$Q_{eqv} = \omega_c \frac{\sum_{i=1}^N W_i}{\sum_{i=1}^N P_{T_i}} = \omega_c \frac{W_T}{P_{T\pi}} \quad (7)$$

where

- Q_{eqv} - Composite Q.
- W_i, P_{Ti} - Energy in and power lost to eigenmode i.
- P_{TT} - Total net power transmitted into the cavity.
- W_T - Total energy stored in all eigenmodes.
- ω_c - Some characteristic frequency.

If the energy in each eigenmode is approximately equal, the following relationship can be derived from the above composite Q equation:

$$\frac{1}{Q_{eqv}} = \frac{1}{N} \sum_{i=1}^N \frac{1}{Q_i} \quad (8)$$

This appears to be the approach used in NBS Technical Note 1066 [Ref. 4]. By considering the wave number $k_r = \omega_i/c$ to be a continuous function of three continuous variables, m, n, and p which correspond to the integers m, n, and l in Equation 4 above, they construct a lattice sum of individual Q values for a wave propagating in the z direction within a cavity (as oriented in Fig. 4). This is accomplished by integrating over the volume of a spherical

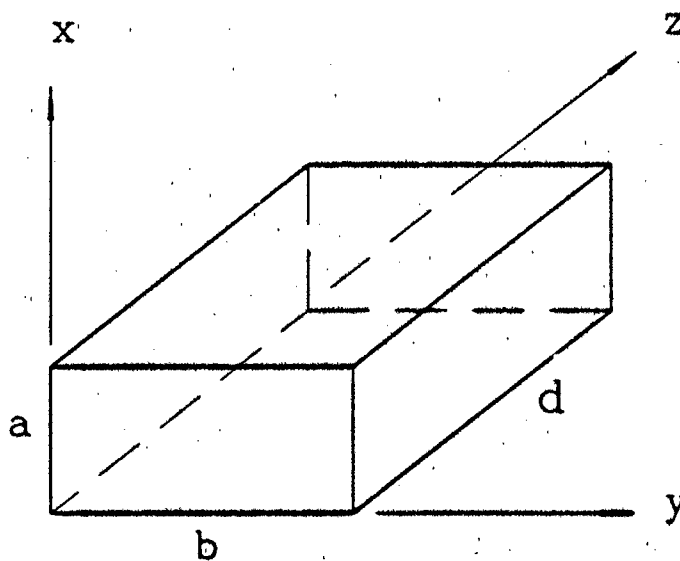


Figure 4. Cavity orientation used to derive fields (from Ref. 4).

shell in the first octant that has an inner radius k and an outer radius $k+\Delta k$. Thus all positive values of m , n , and p are included that satisfy the equation:

$$k_r = \sqrt{\left(\frac{m\pi}{a}\right)^2 + \left(\frac{n\pi}{b}\right)^2 + \left(\frac{p\pi}{d}\right)^2} ; k \leq k_r \leq k+\Delta k \quad (9)$$

The following result was obtained [Ref. 4]:

$$Q = \frac{V}{S \delta_s \mu_r} \frac{3}{2} \frac{1}{1 + \frac{3\pi}{8k} \left(\frac{1}{a} + \frac{1}{b} + \frac{1}{d} \right)} \quad (10)$$

[Note: the relative permeability of the cavity walls, μ_r , was added to correct a typo and the variable "c" as presented in the reference was changed to "d" to avoid confusion with the speed of light constant used above.]

where

- V - Volume of the cavity.
- S - Total internal surface area of the cavity walls.
- δ_s - Skin depth of cavity walls.

Equation 10 appears not to be usable for the definition of composite Q desired for this experiment. This is primarily because only two sets of modes were used in the calculation and the zero order modes seem to have been given undue weighting. These considerations will be discussed as part of the following analysis.

To completely describe the fields within a rectangular cavity, all six types of modes ($TE^{(z)}$, $TM^{(z)}$, $TE^{(x)}$, $TM^{(x)}$, $TE^{(y)}$, and $TM^{(y)}$) must be considered. The composite Q will then be calculated by substituting the power lost to the walls and the energy stored by each mode into Equation 7. Then, an expression will be derived for the net Q which will include power losses to receiving antenna and B-dot probes. With minor modification, the $TE^{(z)}$ and $TM^{(z)}$ modes from NBS Technical Note 1066 [Ref. 4] can be described as presented in Equations 11 and 12.

TE^(z) Modes:

$$\begin{aligned}
E_z &= 0 \\
E_x &= k_y \cos(k_x x) \sin(k_y y) \sin(k_z z) \\
E_y &= -k_x \sin(k_x x) \cos(k_y y) \sin(k_z z) \\
H_z &= 1/(j\eta k_r) k_{xy}^2 \cos(k_x x) \cos(k_y y) \sin(k_z z) \\
H_x &= -1/(j\eta k_r) k_x k_z \sin(k_x x) \cos(k_y y) \cos(k_z z) \\
H_y &= -1/(j\eta k_r) k_y k_z \cos(k_x x) \sin(k_y y) \cos(k_z z)
\end{aligned} \tag{11}$$

TM^(z) Modes:

$$\begin{aligned}
E_z &= \eta/(jk_r) k_{xy}^2 \sin(k_x x) \sin(k_y y) \cos(k_z z) \\
E_x &= -\eta/(jk_r) k_x k_z \cos(k_x x) \sin(k_y y) \sin(k_z z) \\
E_y &= -\eta/(jk_r) k_y k_z \sin(k_x x) \cos(k_y y) \sin(k_z z) \\
H_z &= 0 \\
H_x &= k_y \sin(k_x x) \cos(k_y y) \cos(k_z z) \\
H_y &= -k_x \cos(k_x x) \sin(k_y y) \cos(k_z z)
\end{aligned} \tag{12}$$

where k_r , k_x , k_y , k_z , and k_{xy} have the same significance as in Reference 4 and η is the intrinsic impedance of the medium filling the cavity. That is:

$$\begin{aligned}
k_x &= \frac{m\pi}{a}, \quad k_y = \frac{n\pi}{b}, \quad k_z = \frac{l\pi}{d}, \\
k_{xy} &= \sqrt{k_x^2 + k_y^2}, \quad k_r = \sqrt{k_x^2 + k_y^2 + k_z^2}
\end{aligned} \tag{13}$$

The x and y modes can be easily determined by noting that when the enclosure is rotated as shown in Figure 5, the following transformations occur:

| | |
|--------------|--------------|
| z to x modes | z to y modes |
| z-x | z-y |
| x-y | y-x |
| y-z | x-z |

(14)

Applying Equation 14 to Equations 11 and 12, the other TM and TE modes are:

TE^(x) Modes:

$$\begin{aligned}
E_x &= 0 \\
E_y &= k_z \sin(k_x x) \cos(k_y y) \sin(k_z z) \\
E_z &= -k_y \sin(k_x x) \sin(k_y y) \cos(k_z z) \\
H_x &= 1/(j\eta k_r) k_{yz}^2 \sin(k_x x) \cos(k_y y) \cos(k_z z) \\
H_y &= -1/(j\eta k_r) k_y k_x \cos(k_x x) \sin(k_y y) \cos(k_z z) \\
H_z &= -1/(j\eta k_r) k_z k_x \cos(k_x x) \cos(k_y y) \sin(k_z z)
\end{aligned} \tag{15}$$

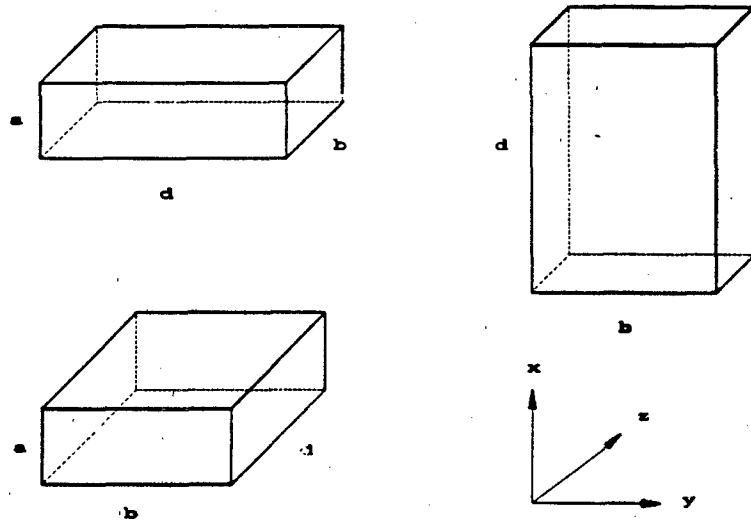


Figure 5. Three different directions of propagation.

TM^(x) Modes:

$$\begin{aligned}
 E_x &= \eta / (jk_z) k_y^2 \cos(k_x x) \sin(k_y y) \sin(k_z z) \\
 E_y &= -\eta / (jk_z) k_y k_x \sin(k_x x) \cos(k_y y) \sin(k_z z) \\
 E_z &= -\eta / (jk_z) k_z k_x \sin(k_x x) \sin(k_y y) \cos(k_z z) \\
 H_x &= 0 \\
 H_y &= k_z \cos(k_x x) \sin(k_y y) \cos(k_z z) \\
 H_z &= -k_y \cos(k_x x) \cos(k_y y) \sin(k_z z)
 \end{aligned} \tag{16}$$

TE^(y) Modes:

$$\begin{aligned}
 E_y &= 0 \\
 E_x &= k_x \sin(k_x x) \sin(k_y y) \cos(k_z z) \\
 E_z &= -k_z \cos(k_x x) \sin(k_y y) \sin(k_z z) \\
 H_y &= 1 / (j\eta k_z) k_x^2 \cos(k_x x) \sin(k_y y) \cos(k_z z) \\
 H_x &= -1 / (j\eta k_z) k_z k_y \cos(k_x x) \cos(k_y y) \sin(k_z z) \\
 H_z &= -1 / (j\eta k_z) k_x k_y \sin(k_x x) \cos(k_y y) \cos(k_z z)
 \end{aligned} \tag{17}$$

TM^(y) Modes:

$$\begin{aligned}
E_y &= \eta / (jk_z) k_{xx}^2 \sin(k_x x) \cos(k_y y) \sin(k_z z) \\
E_z &= -\eta / (jk_z) k_x k_y \sin(k_x x) \sin(k_y y) \cos(k_z z) \\
E_x &= -\eta / (jk_z) k_x k_y \cos(k_x x) \sin(k_y y) \sin(k_z z) \\
H_y &= 0 \\
H_z &= k_x \cos(k_x x) \cos(k_y y) \sin(k_z z) \\
H_x &= -k_z \sin(k_x x) \cos(k_y y) \cos(k_z z)
\end{aligned} \tag{18}$$

where

$$k_{yz} = \sqrt{k_y^2 + k_z^2}, \quad k_{xz} = \sqrt{k_x^2 + k_z^2} \tag{19}$$

Now that at all six types of modes have been defined, it can be noted that the TE and TM are orthogonal in time. That is:

$$\int_0^T \vec{E}^{(TM)} \cdot \vec{E}^{(TM)} dt = \int_0^T \vec{H}^{(TM)} \cdot \vec{H}^{(TM)} dt = 0 \tag{20}$$

where T is the period. The fields for the three directions are not, however, orthogonal for a given polarization. Thus, when calculating the power lost to the walls and the energy stored in the cavity, the TE and TM modes may be treated separately, but the fields for the x, y, and z directions must be added vectorially within the TM or TE mode set. Hence:

TE^(x,y,z) Modes:

$$\begin{aligned}
E_x &= (k_y - k_z) \cos(k_x x) \sin(k_y y) \sin(k_z z) \\
E_y &= (k_z - k_x) \sin(k_x x) \cos(k_y y) \sin(k_z z) \\
E_z &= (k_x - k_y) \sin(k_x x) \sin(k_y y) \cos(k_z z) \\
H_x &= 1 / (j\eta k_z) (k_{yz}^2 - k_x k_y - k_x k_z) \sin(k_x x) \cos(k_y y) \cos(k_z z) \\
H_y &= 1 / (j\eta k_z) (k_{xz}^2 - k_x k_y - k_y k_z) \cos(k_x x) \sin(k_y y) \cos(k_z z) \\
H_z &= 1 / (j\eta k_z) (k_{xy}^2 - k_x k_z - k_y k_z) \cos(k_x x) \cos(k_y y) \sin(k_z z)
\end{aligned} \tag{21}$$

TM^(x,y,z) Modes:

$$\begin{aligned}
E_x &= \eta / (jk_z) (k_{yz}^2 - k_x k_y - k_x k_z) \cos(k_x x) \sin(k_y y) \sin(k_z z) \\
E_y &= \eta / (jk_z) (k_{xz}^2 - k_x k_y - k_y k_z) \sin(k_x x) \cos(k_y y) \sin(k_z z) \\
E_z &= \eta / (jk_z) (k_{xy}^2 - k_x k_z - k_y k_z) \sin(k_x x) \sin(k_y y) \cos(k_z z) \\
H_x &= (k_y - k_z) \sin(k_x x) \cos(k_y y) \cos(k_z z) \\
H_y &= (k_z - k_x) \cos(k_x x) \sin(k_y y) \cos(k_z z) \\
H_z &= (k_x - k_y) \cos(k_x x) \cos(k_y y) \sin(k_z z)
\end{aligned} \tag{22}$$

The power lost to the cavity walls, for small losses, can be calculated using the perturbation method [Ref. 2]:

$$P^c = \frac{R_s}{2} \int_S |\vec{H}_t|^2 dS \quad (23)$$

where R_s is the surface resistance of the cavity walls and H_t is the components of H tangent to the wall surfaces. Applying Equation 23 to Equations 21 and 22, the power lost at all six walls to the TE and TM modes is:

$$P_{TE}^c = \frac{A_{TE}^2 R_s}{4\eta^2 k_r^2} [(ab+ad)(k_{yz}^2 - k_x k_y - k_x k_z)^2 + (ab+bd)(k_{xz}^2 - k_y k_x - k_y k_z)^2 + (ad+bd)(k_{xy}^2 - k_x k_z - k_y k_z)^2]$$

$$P_{TM}^c = \frac{A_{TM}^2 R_s}{4} [(ab+ad)(k_y - k_x)^2 + (ab+bd)(k_x - k_z)^2 + (ad+bd)(k_x - k_y)^2] \quad (24)$$

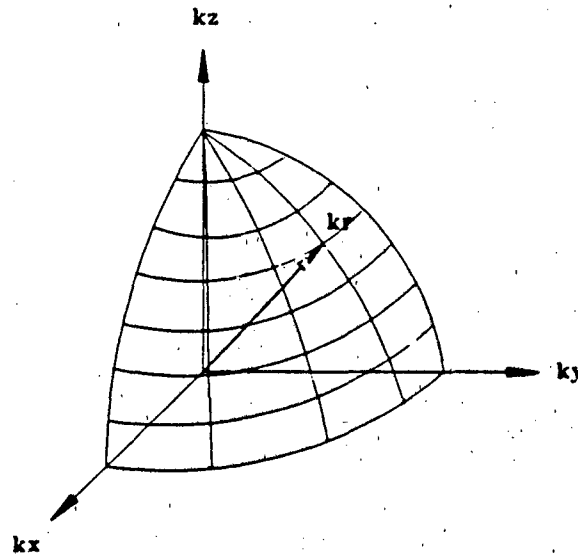


Figure 6. Surface of constant k_r .

The different amplitudes, A_{TE} and A_{TM} , for the TE and TM modes were added to indicate that the amplitudes of the polarizations as defined above may not be equal. Now the k_x , k_y , and k_z dependency can be reduced to strictly a k_r dependency by assuming that the lattice spacing is small compared to k_r and

equal. Now the k_x , k_y , and k_z dependency can be reduced to strictly a k_r dependency by assuming that the lattice spacing is small compared to k_r and therefore can be treated as a continuous function of k_r . Thus by integrating over the surface defined by $k = k_r$ (Fig. 6) in spherical coordinates, the power lost to the walls is:

$$\begin{aligned} P_{TE}^c &= \frac{A_{TE}^2 R_s}{12\eta^2} k_r^4 (\pi-2) S \\ P_{TM}^c &= \frac{A_{TM}^2 R_s}{12} k_r^4 (\pi-2) S \\ P^c &= P_{TE}^c + P_{TM}^c = \frac{A^2 R_s}{12\eta^2} k_r^4 (\pi-2) S \end{aligned}$$

where

$$S = 2(ab+ad+bd), \quad A^2 = A_{TE}^2 + \eta^2 A_{TM}^2 \quad (25)$$

The energy stored in the cavity for any eigenmode can be found from [Ref. 2]:

$$W = \frac{\epsilon}{4} \int_V \vec{E} \cdot \vec{E} dV + \frac{\mu}{4} \int_V \vec{H} \cdot \vec{H} dV = \frac{\epsilon}{2} \int_V \vec{E} \cdot \vec{E} dV = \frac{\mu}{2} \int_V \vec{H} \cdot \vec{H} dV \quad (26)$$

thus

$$\begin{aligned} W_{TE} &= \frac{V \epsilon A_{TE}^2}{16} [(k_y - k_z)^2 + (k_z - k_x)^2 + (k_x - k_y)^2] \\ W_{TM} &= \frac{V \mu A_{TM}^2}{16} [(k_y - k_z)^2 + (k_z - k_x)^2 + (k_x - k_y)^2] \end{aligned}$$

where

$$V = abd \quad (27)$$

Again, keeping $k = k_r$ constant and integrating over the spherical surface:

$$\begin{aligned} W_{TE} &= \frac{V \epsilon_0 A_{TE}^2}{16} k_r^4 (\pi-2) \\ W_{TM} &= \frac{V \mu_0 A_{TM}^2}{16} k_r^4 (\pi-2) \\ W &= W_{TE} + W_{TM} = \frac{A^2 V \mu_0}{16\eta^2} k_r^4 (\pi-2) \end{aligned} \quad (28)$$

Substitution in Equation 6 yields:

$$Q_{k_r} = Q_{\overline{TS}, \overline{TK}}^{(x,y,z)} = Q_{\overline{TS}}^{(x,y,z)} = Q_{\overline{TK}}^{(x,y,z)} = \frac{3}{4} \frac{\omega \mu_o V}{R_s S}$$

since

$$R_s = \frac{\omega \mu_o \mu_r \delta_s}{2},$$

and

$$Q_{k_r} = \frac{3}{2} \frac{V}{\mu_r S \delta_s} \quad (29)$$

where μ_r and δ_s are respectively the relative permeability and skin depth of the walls.

Even though the variation of k_r over the interval $k \leq k_r \leq k+\Delta k$ has not yet been considered, as promised earlier, the justification for not treating the zero order modes separately (as was the case in Ref. 4) can now be provided.

Consider in the equations for P (Eq. 24) and W (Eq. 27), the integration over the surface was completed in spherical coordinates with the limits of θ and ϕ being $[0, \pi/2]$. The zero order modes lie on the very edges of the surface of integration. It was assumed upfront that the mode density was high enough to consider the surface continuous. Therefore, in the limit, the zero order modes contribute nothing to the surface integral. In Reference 4 the zero order modes, even though there are significantly less of them, are given equal weighting in the sum of the reciprocals. To be less biased, each $1/Q$ value should have been multiplied by the total count of lattice points contributing to that $1/Q$ and the sum then divided by the count of all lattice points in the shell.

Now consider the case when the source pumping the cavity has its power spread out over some spectrum. It is convenient to express this type of signal as a power spectral density. Let the source's power spectral density be $P_r(\omega)$ in W/Hz. Then the total average power and the average power in small interval $P_{\Delta\omega}$ can be found using standard communication theory [Ref. 5]:

$$\begin{aligned}
 P_{TT} &= \frac{1}{2\pi} \int_{-\infty}^{\infty} P_T(\omega) d\omega \\
 P_{\Delta\omega}(\omega) &= \frac{1}{2\pi} P_T(\omega) \Delta\omega \\
 \Delta\omega &< \omega
 \end{aligned}
 \tag{30}$$

For an empty cavity (no loads or receiving devices), the power absorbed by the walls is identical to the net power being transmitted into the cavity. Thus the power lost to the walls, P^l in a small frequency interval is $P_{\Delta\omega}$. Therefore, the energy in a small frequency interval, $\Delta\omega$ can be found by equating Equations 29 and 30 and substituting into Equation 6:

$$\Delta W = \frac{1}{2\pi} \frac{3}{4} \frac{\mu V}{S R_g} P_T(\omega) \Delta\omega \tag{31}$$

Now the composite Q is determined by substituting the above energy expression into Equation 7 and replacing the summations with integrals:

$$Q_{eqv} = \frac{\omega_c \frac{3}{4} \frac{\mu V}{S} \sqrt{\frac{2\sigma_c}{\mu_c \mu_r}} \int_{-\infty}^{\infty} \omega^{-\frac{1}{2}} P_T(\omega) d\omega}{\int_{-\infty}^{\infty} P_T(\omega) d\omega} \tag{32}$$

Clearly, if $P_T(\omega)$ is any arbitrary function, then the composite Q will be highly dependent upon it. But, if instead the spectrum of $P_T(\omega)$ is limited to a narrow bandwidth, BW so that $BW \ll \omega_c$, then it can be easily shown that $Q_{eqv} \approx Q_{tr}$. First consider a definite integral over a small interval about x_c of a generic function $f(x)$ which can be expressed as a convergent power series:

$$\begin{aligned}
 \int_{x_c - \delta/2}^{x_c + \delta/2} f(x) dx &= \int_{x_c - \delta/2}^{x_c + \delta/2} \left[\sum_{i=0}^{\infty} a_i x^i \right] dx \\
 &= \sum_{i=0}^{\infty} \frac{1}{i+1} a_i x_c^{i+1} \left[\left(1 + \frac{\delta}{2x_c}\right)^{i+1} - \left(1 - \frac{\delta}{2x_c}\right)^{i+1} \right]
 \end{aligned}
 \tag{33}$$

The bracketed quantity in the last part of Equation 33 can be expanded as the difference of two binomial series with all the even terms canceling. Then, by discarding all but the first term remaining, the equation can be simplified to:

$$\int_{x_c - \delta/2}^{x_c + \delta/2} f(x) dx = \sum_{i=0}^{\infty} a_i \frac{1}{i+1} x_c^{i+1} \left[(i+1) \frac{\delta}{x_c} \right] = \delta f(x_c) \quad (34)$$

Applying this result to Equation 32, the following result occurs:

$$\int_{\omega_c - BW/2}^{\omega_c + BW/2} \omega^{-\frac{1}{2}} P_t(\omega) d\omega = BW \omega_c^{-\frac{1}{2}} P_t(\omega_c)$$

and

$$\int_{\omega_c - BW/2}^{\omega_c + BW/2} P_t(\omega) d\omega = BW P_t(\omega_c) \quad (35)$$

hence

$$Q_{eqv} = \omega_c \frac{3}{4} \frac{V}{S R_s} = \frac{3}{2} \frac{V}{\mu_r S \delta_s} = Q_k$$

The error introduced by discarding all but the first term of the binomial expansion is highly dependent on the even, higher order derivatives of $f(x)$, i.e.:

$$Error = \sum_{m=1}^{\infty} \frac{1}{2^{2m} (2m+1)!} \delta^{2m} f^{(2m)}(x_c) \quad (36)$$

Hence, as expected, the smoother $f(x)$ is in the vicinity of x_c , the better Equation 35 will approximate the actual integral.

It should also be pointed out that the relative permeability for most materials (including the steels commonly used to construct mode-stir chambers), except ferrites, is ≈ 1 above medium frequencies (300 KHz to 3 MHz) [Ref. 6]. Since proper mode stirring requires a high mode density, useful lower frequency bounds range in the hundreds of megahertz for a typically

sized chamber. Therefore, for most practical purposes, the relative permeability in Equations 29 and 35 can be assumed to be unity.

Thus far only empty, unloaded cavities have been considered. Normally, when the Q of a cavity is being measured, loads in the cavity should not be considered separately. However, experience has shown [Ref. 7] that at the lower end of the spectrum, theoretical calculations for the Q always tend to drastically overestimate the actual Q. A large part of the loading effect that takes place can be attributed to the antennas used to either pump the cavity or to measure the effective power density within the cavity. If the actual net pumping power is measured (incident minus reflected) and used as the reference for the Q calculation, then the transmit antenna can be ignored. However, the receiving antenna must still be accounted for.

The effect of a receiving antenna (horn antenna) on the Q of a cavity can be calculated in a straightforward manner. First, the expected value of the gain of the antenna in a mode-stir chamber is 1. This is intuitively obvious from the fact that all the energy radiating from an antenna must end up on a closed sphere that surrounds it. Additionally, the polarization factor of 1/2 must be accounted for [Ref. 8]. Therefore the effective area of the antenna is:

$$A_e = \frac{\lambda^2}{8\pi} = \frac{\pi}{2k_i^2} \quad (37)$$

The effective power density can be calculated from energy density in the cavity and then combined with Equation 3 to determine the net power lost to the antenna:

$$P_{lost} = A_e P_D = \frac{\pi}{2k_i^2} \frac{WC}{V} \quad (38)$$

The Q of a cavity with perfectly conducting walls but loaded with an antenna is:

$$Q_e = \frac{\omega W}{P_{lost}} = 2 \left(\frac{\omega}{c} \right)^3 \frac{V}{\pi} \quad (39)$$

The same approach can be used to determine the effect of the B-dot probes on the overall Q. First, however, consider that a B-Dot probe measures only the component of the B field normal to the loop surface. Therefore, to determine an equivalent B_n^2 to use in Equation 3 consider a wave incident on the B-Dot at some random angle, θ , relative to the normal vector of the probe's loop, then integrate over all angles to find the average value of B_n^2 . Noting that the projection of the B field on the normal to the loop is related to the cosine of the angle between them:

$$(B_n^2)_{avg} = \frac{1}{\pi} \int_0^\pi B^2 \cos^2 \theta d\theta = \frac{1}{2} B^2 \quad (40)$$

Thus from Equations 3, 6, and 40:

$$Q_b = \frac{100 V}{\mu_o A_o^2 \omega}$$

thus

$$Q_{NT} = \frac{1}{\frac{1}{Q_{eqv}} + N_s \frac{1}{Q_s} + N_b \frac{1}{Q_b}} \quad (41)$$

where N_s and N_b are the number of standard antennae and the number of B-dot probes respectively. It should be noted that the reciprocal of the sum of reciprocals is appropriate because the energy is shared by all the loads in the cavity. This is similar to the Q analysis used to determine the effect of a lossy dielectric on a cavity [Ref. 2].

Figure 7 shows the theoretical Qs due to the lossy cavity walls, a receiving antenna, and four 0.125 cm² per half B-dot probes for the NT enclosure. Even with four B-dot probes (eight half probes), the associated probe Q has little impact on the net Q. On the other hand, at the low frequencies, the receiving antenna can have a significant impact on the net Q. In fact, for a

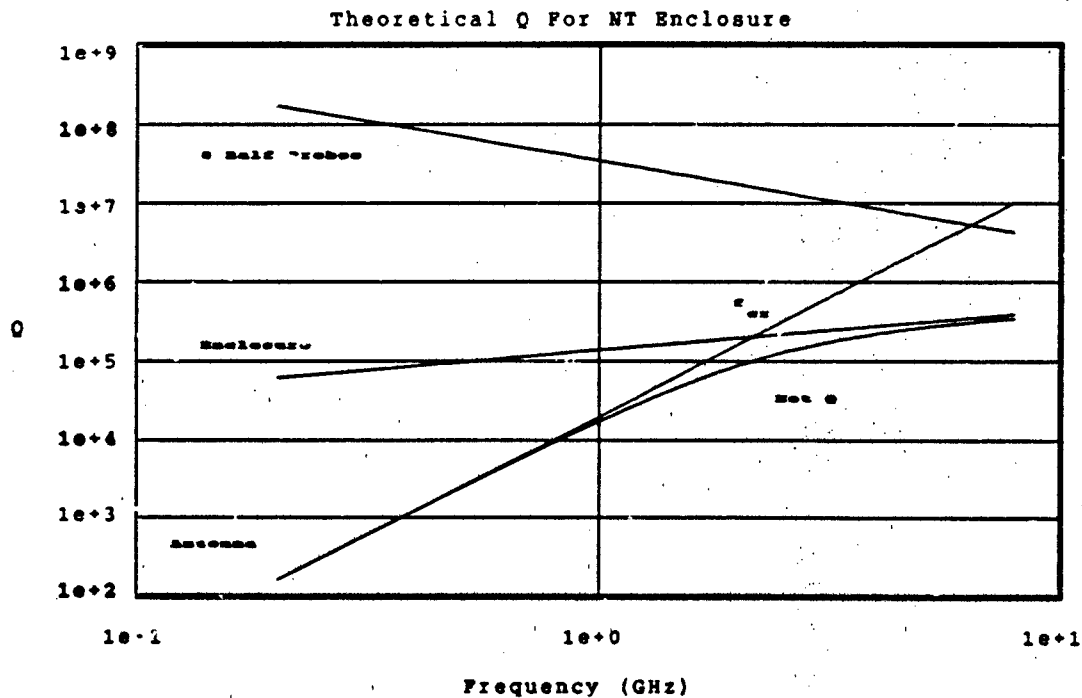


Figure 7. Effect of probes and antenna on the net Q.

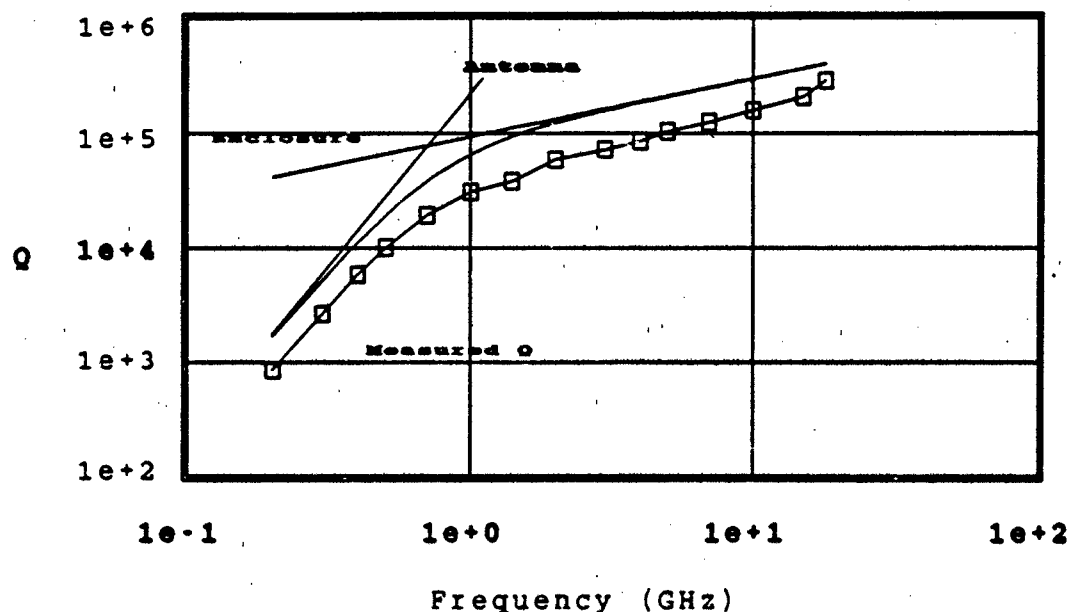
good quality chamber, the net Q measured at the lower frequencies will be almost exclusively due to the antenna. As can be seen from the figure, one can define a minimum critical frequency, f_{cr} where the Q curve due to the antenna and the Q curve due to the lossy walls cross:

$$f_{cr} = \frac{1}{2\pi} \left[\frac{9 \pi^2 \mu_0 \sigma c^4}{32 S^2} N_s^2 \right]^{1/3} \quad (42)$$

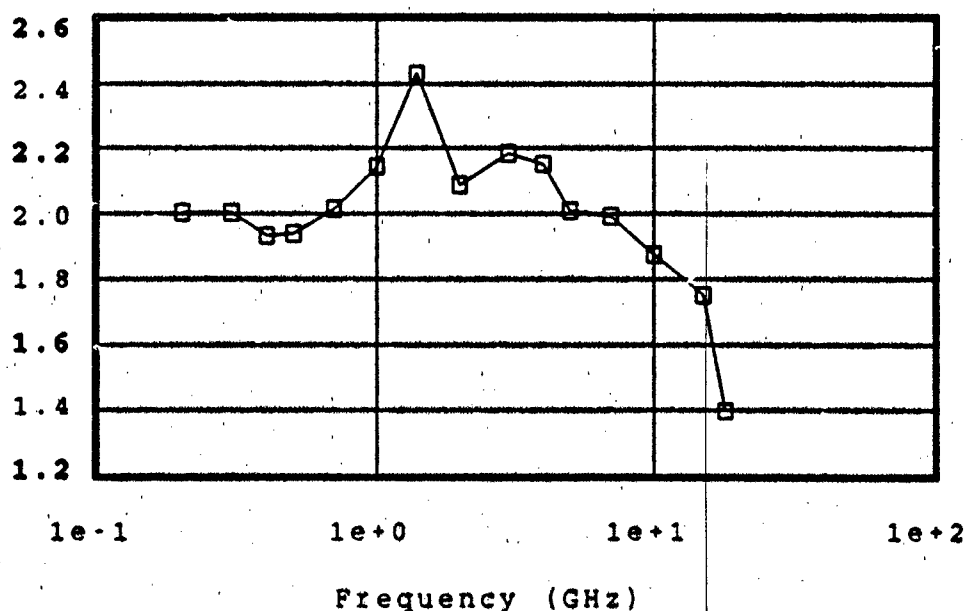
[Note that μ_r was not included in the above expression due to the earlier discussion of it being unity at the typical frequencies, >3 MHz, used in mode-stir chambers and for the typical metals used.]

Thus, well below this frequency the antenna(s) will dominate the net Q, while well above this frequency, the Q for the lossy walls will dominate.

Figure 8 shows the predicted value of the Q , based upon Equations 39 and 41, for the 2.74 X 3.05 X 4.57 m steel NIST chamber as well as the actual measured Q . A complete description of this chamber and how the measurements were made appears in Reference 1. The theoretical model would appear to fit the shape of the experimental data very well all the way up to 18 GHz. There does, however, seem to be a factor of 2 difference between the prediction and the model. This difference appears both in the region where the antenna dominates the Q and where the walls dominate the Q . If the difference appeared only in the latter region, it could be explained away by assuming extraneous loads in the chamber such as dust, test stand material, etc. Because the factor of 2 appears in both regions, though, the source of the error must be common to both Q predictors. The only parameters that Q_a and Q_{eq} have in common are the chamber volume, the source frequency, and of course, the experimental data. It should also be pointed out that above 18 GHz, the experimentally measured Q begins to rapidly exceed the predicted Q . Neither one of these discrepancies are currently explainable and further study is required.



a. Q for NIST Enclosure.



b. Q_{net} / Q_{exp} .

Figure 8. Theoretical and Measured Q for the NIST chamber.
(Experimental data provided courtesy of NIST.)

FREQUENCY STIRRING

PREFERRED METHOD

The conventional method of mode-stirring uses a metallic paddle wheel to continuously or incrementally change the boundary conditions within the reverberation chamber while maintaining a constant pumping frequency. In this manner, field homogeneity is achieved by averaging the contribution of many different eigenfunctions to a given point in the chamber. In the frequency stir method, the boundary conditions are maintained constant while the frequency is allowed to vary over a narrow interval about some center frequency. Then the contribution of each eigenfunction to a given spatial point in the chamber, in that narrow band of frequency, is averaged to provide the field homogeneity. The advantage of the frequency stir method over the mode stir is that by spreading the power over a band of frequency, the eigenfunctions corresponding to that band can be stimulated simultaneously. Thus, because the energy stored in the fields in an arbitrarily small volume centered at any given spatial point is the average of all the energies in the individual eigenmodes, field homogeneity is achieved on a real time basis (this assumes that the mean of the energy density contributed by the eigenmodes, in the narrow band of frequency, to a given point in the chamber is spatially stationary). Real time homogeneity can drastically reduce test times. Even if individual eigenfunctions are changed by adding a test object or moving an existing test object within the chamber, the mean over the frequency band will remain constant (within the limits of the sampling variance).

There are any number of techniques that can be used to provide the source frequency agility required. At minimum, however, the method used should meet the following criteria:

- The power spectrum should be flat across the agility bandwidth to simplify data interpretation.

- The signal should be ergodic (or at least loosely time stationary over the maximum averaging period of the test article and/or the power measuring instrument) so that real time homogeneity can be achieved.
- The center frequency and bandwidth agility of the source should be variable over a wide parameter set to facilitate test flexibility.
- The average output power should be continuously variable or variable in 3 dB or less increments, from 1 W to at least 200 W to allow for a wide range of cavity quality factors and test article upset levels.

The method chosen for this experiment uses band limited white Gaussian noise (WGN) up-converted by performing double sideband, suppressed carrier modulation with an RF signal from a synthesized sweeper. The output is then amplified with a TWT amplifier to meet the higher power level requirements. Center frequencies between 0.5 and 18 GHz and frequency agile bandwidths of 10, 20, 50, and 100 MHz can be easily realized. In addition, the power output from the sweeper can be varied in 1-dB increments from -120 dBm to $\approx +15$ dBm. Therefore, for all practical purposes, the dynamic range of the technique is identical to the dynamic range of the amplifier. Figure 9 demonstrates the theoretical spectrum of the signal at each stage of the signal processing. The synthesized sweeper is used to generate the monochromatic signal which determines the center frequency of the output while the WGN source and low pass filters provide the frequency agility. One of the convenient properties of WGN is that it will maintain its statistical properties after having passed through a linear, invariant system such as a low pass filter [Ref. 5].

Figure 10 shows the actual output at a fixed center frequency of 1.5 GHz, immediately after up-conversion, of the technique as measured by a spectrum analyzer.

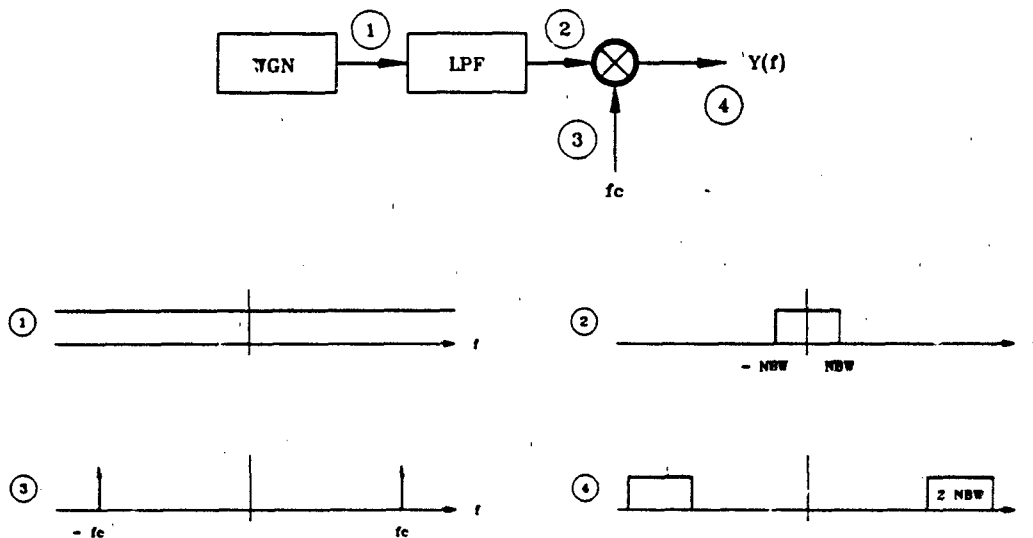


Figure 9: Frequency stir spectrum.

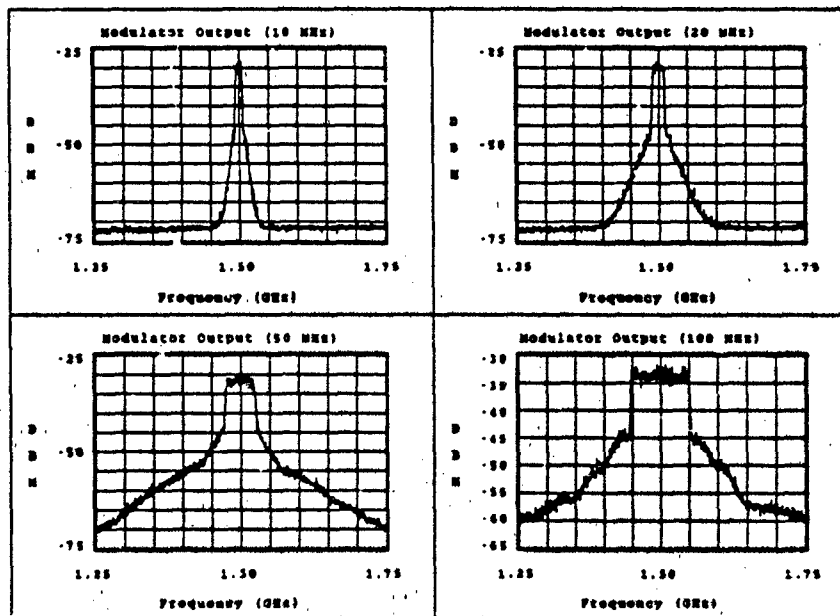


Figure 10. Output of the up-converters for a center frequency of 1.5 GHz and all four agility bandwidths.

FIELD HOMOGENEITY PREDICTIONS

If one assumes that the energy density at an arbitrary point within the reverberation chamber, due to any given eigenmode, is a random variable (this assumption is based on convenience not fact), e_i with definable statistics, then the variation of the mean E_j of a sample of n eigenmodes can be described using simple sample theory [Ref. 9]:

$$\sigma_E = \frac{\sigma_e}{\sqrt{N}} \quad (43)$$

where σ_e and σ_E are the standard deviation of the random variables e and E respectively (it is assumed that the sample size N is small compared to the total sample space). The sample size, N can be determined directly from the mode density (Eq. 5) as function of the agility bandwidth, BW and the center frequency, f_c . Hence:

$$\sigma_E = \frac{\sigma_e}{2 f_c} \sqrt{\frac{c^3}{2\pi V BW}} \quad (44)$$

Further, the standard deviation of e can be approximated by considering the energy density due to an individual eigenfunction to be a random variable which is a function of a random spatial coordinate (X,Y,Z) .

Let X , Y , and Z be independent random variables, each uniformly distributed on $[0,1]$, i.e.:

$$\begin{aligned} f_X(x) &= 1; & 0 \leq x \leq 1 \\ f_Y(y) &= 1; & 0 \leq y \leq 1 \\ f_Z(z) &= 1; & 0 \leq z \leq 1 \end{aligned} \quad (45)$$

Their joint distribution is:

$$f(x,y,z) = f_X(x)f_Y(y)f_Z(z) = 1 \quad (46)$$

Thus, the point (X,Y,Z) will represent a random point within a one cubic unit of space with the probability of selecting any point in that volume being equal. Now consider a small volume inside a rectangular cavity in which a single eigenfunction is stimulated. Further, let the spatial coordinates be chosen within the small volume so that the volume encompasses exactly one spatial period of the eigenfunction in a unit cube. A normalized function, $g(X,Y,Z)$ expressing the energy density pattern as a function of the random variables X, Y, and Z is:

$$g(X,Y,Z) = \sin^2\left(\frac{\pi}{2}X\right) \sin^2\left(\frac{\pi}{2}Y\right) \sin^2\left(\frac{\pi}{2}Z\right) \quad (47)$$

The expected value and variance of g can be easily determined [Ref. 10]:

$$\begin{aligned} \mu_g &= E[g(X,Y,Z)] = \int_0^1 \int_0^1 \int_0^1 g(x,y,z) f(x,y,z) dx dy dz = \frac{1}{8} \\ \sigma_g^2 &= E\{[g(X,Y,Z) - E[g(X,Y,Z)]]^2\} = \frac{19}{512} \end{aligned} \quad (48)$$

After scaling the variance with the amplitude of the energy density, the standard deviation of a single, randomly sampled eigenfunction is determined:

$$\sigma_s = w \sigma_g = \frac{8W}{V} \sigma_g = \frac{W}{V} \sqrt{\frac{19}{8}} = \frac{Q P_T}{2\pi f V} \sqrt{\frac{19}{8}} \quad (49)$$

Substitution directly into Equation 44 yields:

$$\sigma_s = \frac{Q P_T}{16f^2} \sqrt{\frac{19c^3}{\pi^3 V^3 BW}} \quad (50)$$

It should be noted that the Q in the above equation should be considered a net Q as defined earlier. However, by substitution of only the theoretical Q from Equation 35, the deviation's dependence on the frequency and cavity dimensions can be determined for the ideal cavity:

$$\sigma_E = \frac{3 P_T}{32 S} \sqrt{\frac{19 \mu_o \sigma c^3}{\pi^2 \mu_r V BW f^3}} \quad (51)$$

[The conductivity, σ , under the square root sign should not be confused with the standard deviation symbol.]

At first glance, it would seem that an easy way to improve the homogeneity of the fields in a given cavity would be to simply increase the surface area, S , by corrugating the walls or maybe increasing the volume. This would in fact work, but at the expense of the maximum field levels achievable with a given P_T . Clearly, though, increasing the agility bandwidth, BW , or the frequency, f , will improve the field homogeneity without sacrificing field amplitudes. Although Equation 51 is useful for investigating the energy density homogeneity's frequency and bandwidth dependence, it is desirable to formally define a homogeneity parameter that is independent of the power pumped into the cavity and thus the amplitude of the energy density within. A simple definition (and one that is commonly used), yet one that can easily be determined experimentally, is the maximum average energy density divided by the minimum energy density (or power density) measured in the cavity, expressed in decibels, i.e.:

$$\psi = 10 \log \frac{W_{max}}{W_{min}} = 10 \log \frac{P_{dn_{max}}}{P_{dn_{min}}} \quad (52)$$

It is difficult, however, to use statistics to predict maxima and minima of data sets when the density function is not known. There are techniques that can be employed to calculate the density function from Equation 47 and Equation 52, albeit most are very difficult. Therefore, the preferred technique is that of Monte Carlo simulation. Using Equation 47, N random

Table 1. Standard deviation of field ratios for different values of N.

Monte Carlo Simulation of Field Homogeneity

| N | σ | N | σ | N | σ |
|----|----------|-----|----------|------|----------|
| 2 | 11.35 | 16 | 2.54 | 350 | 0.515 |
| 3 | 8.47 | 18 | 2.35 | 600 | 0.380 |
| 4 | 6.58 | 20 | 2.23 | 850 | 0.323 |
| 5 | 5.61 | 25 | 2.03 | 1100 | 0.286 |
| 6 | 4.72 | 29 | 1.84 | 1350 | 0.260 |
| 7 | 4.49 | 35 | 1.65 | 1600 | 0.238 |
| 8 | 3.88 | 45 | 1.46 | 1850 | 0.220 |
| 10 | 3.47 | 57 | 1.26 | 2100 | 0.200 |
| 12 | 3.15 | 82 | 1.02 | 2350 | 0.190 |
| 14 | 2.84 | 100 | 0.934 | 2600 | 0.186 |

field values can be produced and averaged by using three randomly generated values for X, Y, and Z. This is done twice, and the ratio is saved in decibels. This is repeated for a large number of points (2000-5000 in this simulation) and then the standard deviation is calculated using the usual methods. Table 1 lists the standard deviation for several different values of N. Not knowing the density function for Equation 52, relating the standard deviation in Table 1 to Equation 52 is not possible. If it is assumed a priori that the data are normally distributed (evidence of this will be provided later), then a rule of thumb criterion can be established. For example, to determine a level in which 99 percent of the magnitude of the ratio data will be $> \psi_{0.99}$, 2 1/2 standard deviations can be used (\approx 99 percent of the area under the normal distribution falls between ± 2 1/2 standard deviations) to predict the experimental results. The selection of the 99 percent threshold is arbitrary, but, as will be seen in the results, seems to relate the measured standard deviation to the measured homogeneity very well, i.e., $\psi = 2.5 \sigma$. For example, if one desires a homogeneity of 3 dB, then from Table 1, at least 57 modes would need to be stimulated simultaneously.

Now the agility bandwidths required to achieve the same field uniformity results as achieved by the conventional paddle wheel technique used in a full size chamber such as the NIST chamber mentioned in the introduction can be predicted. As stated earlier, field uniformities of $< \pm 3$ dB above 1 GHz and $< \pm 2$ dB above 2 GHz were achieved for the 40 m³ chamber. Using the 99 percent rule of thumb discussed above, 57 modes would be required for above 1 GHz and somewhere in the neighborhood of 200 modes would be required above 2 GHz. Applying Equation 5, the agility bandwidths can be calculated as ≈ 1.5 MHz and 1.3 MHz for the 1 GHz and 2 GHz range, respectively. Of course this is an ideal situation, and therefore a more reasonable estimate is probably in the area of 5 MHz.

COUPLING CROSS SECTIONS

One of the fundamental motivations for conducting low power microwave tests is to determine inexpensively a system or subsystem's coupling cross section or effective area. Cross section is defined as [Ref. 11]:

$$\sigma(f) = \frac{P_L(f)}{S_{inc}(f)} = \frac{\eta_o |H_v(f)|^2}{R_L} \quad (53)$$

where:

$\sigma(f)$ - Coupling cross section.

P_L - Power delivered to the measuring instrument.

$H_v(f)$ - Voltage transfer function (voltage impressed at the test point divided by the magnitude of the incident E field).

R_L - Input impedance of the measuring instrument.

$S_{inc}(f)$ - Power density incident on the system.

The first observation that can be made about Equation 53 is that it assumes that the test object is being radiated with a plane wave. Secondly, it also

assumes that the source of radiation is at a single frequency. Neither of these assumptions are correct in the case of frequency stirring. As discussed earlier, a B-dot probe inside a cavity with an isotropic field, will measure 1/2 of the power density associated with a wave traveling in a single direction that is properly oriented to the probe. If you consider a point inside this cavity with isotropic fields, then the power density impinging on that point will continuously change direction, yet the average magnitude of the power density will remain constant and, as mentioned, will be twice that measured by a B-dot. For lack of a better term, this power density will be called fringe power density (borrowed from microwave oven terminology). Now consider the surface of a large test object; the power incident on the surface is now limited to 2π steradians. If one is simply interested (when studying heating effects, for example) in the average power density falling on the surface (call it surface power density) it can be calculated as:

$$P_s = \frac{1}{\pi} \int_0^{\pi/2} P_f \cos\theta \, d\theta = \frac{1}{\pi} P_f \quad (54)$$

Where P_s and P_f are the surface and fringe power densities respectively. However, when studying the coupling due to a port of entry (POE), the expected value of the directivity will always be one. However, the polarization factor will vary from POE to POE.

In the case of subsystem which would normally exist in an equipment bay or cavity, it makes sense to use the fringe power density when determining cross sections because this is typically what is used when measuring the shielding effectiveness of the full-up system. In other words, the full-up object is illuminated with a plane wave while the fringe power density is measured within the cavity. The ratio of the two then relates the fringe power density within the cavity to the plane wave. Thus, cross sections measured relative to the fringe power density can be related directly to power density incident on the full-up system. A question immediately arises, however, if the coupling cross section at a given circuit node within a full-up system is measured in a reverberation chamber, how can this information be related to plane wave illumination in an anechoic chamber, for example? If the cross section for a full-up system is measured relative to the fringe power

density, then this is equivalent to radiating the test object in an anechoic chamber with a power density at target equivalent to the fringe power density from many different directions with many different polarizations and then averaging the results. Another useful way of interpreting the cross section as measured in chamber would be as the expected value of the cross section that would occur if the target was shot at from a random direction with a random polarization.

So far only the effect of isotropic illumination on the cross section has been discussed. The effect of spreading the spectrum of the pumping source will now be considered.

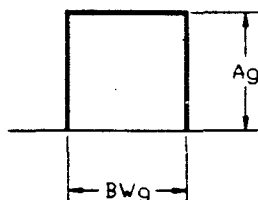
Because the measuring instrument effectively measures the total average power being received by the probe over the agility bandwidth, measuring the cross section using this method is equivalent to convoluting a gating function with the narrow band cross section and then dividing by the fringe power density, i.e.:

$$\sigma_{fs}(f) = \frac{\int_{f_c - BW/2}^{f_c + BW/2} \Pi(f') \sigma(f' - f) df'}{\int_{f_c - BW/2}^{f_c + BW/2} \Pi(f) df} \quad (55)$$

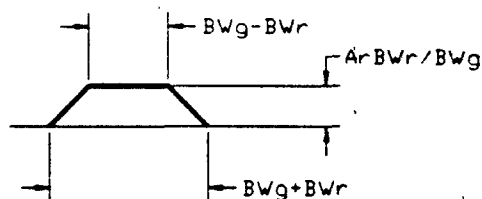
This has the same effect as mathematically smoothing $\sigma(f)$ over the same bandwidth. The primary difference is, however, that the smoothing is done in a real time manner and is independent of the sampling resolution. In other words, if the sample interval was greater than the smoothing window, mathematical smoothing would not work and this method would.

As shown in Figures 11 and 12, details in the cross section that span frequency intervals less than the agility bandwidth will tend to be washed out, while those that span greater intervals will remain. In fact, when the bandwidth of the resonance is less than the bandwidth of the source pumping the cavity, the resonance will be reduced by the ratio of the resonance to the source bandwidth. This may create a problem if the test asset has coupling resonances with bandwidths smaller than the agility bandwidth

GATING FUNCTION



CONVOLUTION/ $(A_g BW_g)$



CROSS SECTION

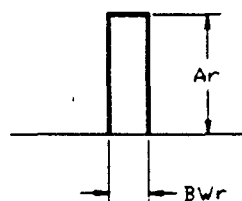
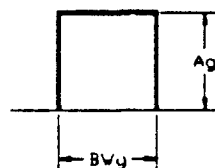
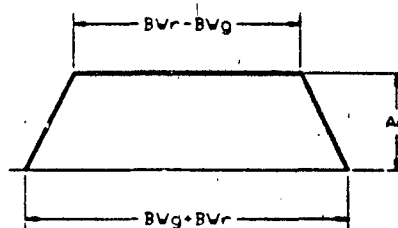


Figure 11. Measured cross section when the bandwidth of resonance is smaller than the bandwidth of the gating function.

GATING FUNCTION



CONVOLUTION/ $(A_g BW_g)$



CROSS SECTION

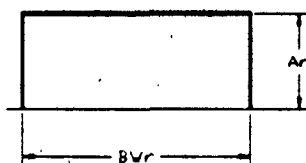


Figure 12. Measured cross section when the bandwidth of resonance is greater than the bandwidth of the gating function.

required to maintain adequate stirring. Typically, however, test object resonances less than a few tens of megahertz are due to the modes set up in the test article itself. These resonances are normally of little interest because of their dependence on the finer details of the test asset. For example, if a cable run on one aircraft is slightly different than another of the same type, drastic differences can be realized in the details of the cross section even though the trend data remain the same. Objects as insignificant as an aluminum soda container can make significant differences in the frequencies at which these narrow resonances occur.* Except for the introduction of some ambiguity at the band edges, the wider, POE resonances will pass through this technique unscathed, as can be seen from the amplitude of the resulting convolution in Figure 12.

SHIELDING EFFECTIVENESS

Shielding effectiveness (SE) is a dimensionless quantity which relates the fields measured inside a test object to those that would be measured if the test object were not present and can be experimentally measured by simply measuring the fields in the test object using a probe and then dividing that by the free field measurement made with the same probe. When doing this measurement using the frequency stir technique, the considerations that were made for the coupling cross section measurement must also be made for the shielding effectiveness measurement. That is, the resulting information obtained is an average or expected value over many angles of incidence and polarizations, and the data are convoluted with the pumping source function.

UPSET THRESHOLD TESTING

One of the most useful applications of reverberation chamber testing is its use to determine the threshold for electromagnetic upset of a unit under test. This is primarily because very large field levels can be achieved in these chambers using modestly low power driving sources. In the conventional paddle wheel mode-stir chamber, upset testing can be a lengthy process.

*Price, R., et al. The Pepsi Syndrome as it Applies to High Power Microwave Susceptibility Analysis, JAYCOR. Albuquerque, NM, August 1990. (Unpublished).

because for each power level attempted, the paddle wheel must be rotated through many positions at a rate less than the test object's response rate. Once the lowest power level in which an upset occurs is recorded, the power density in the chamber can be measured. The difficulty, however, in interpreting these results is that when the upset occurs, there is at no time a truly uniform field within the chamber. In other words, the front of the test object may be in a hot spot and the rear of the object may be in a cold spot when the upset takes place. The frequency stir method eliminates this ambiguity by providing a real time homogenous, isotropic field. Also, because the field is the same throughout the chamber, the power density can be monitored while the source power is slowly raised until an upset occurs.

There is one point that should be noted when using the frequency stir technique to cause upset. That is the fact that the signal being received by the unit under test contains up-converted noise that when detected by the test object may be in-band of the object's electronics. In the paddle wheel method, the detected signal is just a DC level. The unit under test may respond differently to a noisy signal than to a DC signal. The frequency stir upset method was successfully used on an aircraft subsystem. Testing was completed in <5 minutes. The results of the test are not included here due to their security classification and the fact that there currently are no other data available on this device for comparison.

TEST CONFIGURATIONS

FIELD UNIFORMITY SWEPT MEASUREMENTS (NT Enclosure)

Figure 13 shows the general test setup used to conduct the field uniformity tests for the NT enclosure. Four B-dot (JAYCOR TLB-3, 8 GHz, 0.125 cm²/half) probes were placed at different locations within the reverberation chamber. As depicted in Figure 14, they were placed in random locations with all three orientations (x,y, and z) represented. A three-dimensional schematic of the NT reverberation chamber appears in Figure 1. As shown, it is a 6 x 4 x 5 ft welded aluminum enclosure with three 2 x 2 ft access panels with RF gaskets and secured with bolts every 3 in around their perimeter. The microwave launch into the cavity is accomplished using a broad band (1 to 18 GHz) horn positioned at nonorthogonal angles to the cavity wall to facilitate multiple mode excitation. Equipment control and data acquisition are facilitated via a 486 computer using a National Instruments GPIB board. The HP83620A Synthesized Sweeper provides the user selected frequency range and power level to the up-converter bank. Though not shown in Figure 13, external level control was provided via a coupler and HP423B Crystal Detector placed at the output of the TWT bank. External leveling was used to maintain the TWTs at an output power level of ≈ 43 dBm. This helped to minimize TWT harmonic distortion and protect other equipment in the system from being damaged by excessive power.

The frequency agility is provided by the NC7907 Noise Source. The noise source's bandwidth and output power can be set by the 486 computer. In order to vary the maximum 100-MHz bandwidth output, the noise source has four user selectable internal low pass filters (5, 10, 25, and 50 MHz). Further, the maximum output power of 30 dBm can be varied via an internal programmable attenuator. The control software developed for this experiment automatically selects the appropriate filter and attenuator value based upon the desired agility bandwidth for the test at hand. The up-converter bank provides double sideband, suppressed carrier modulation of the microwave carrier by the band limited WGN. Due to the double sideband nature of the modulation, the output of the up-converter bank has twice the bandwidth of the output of the noise source.

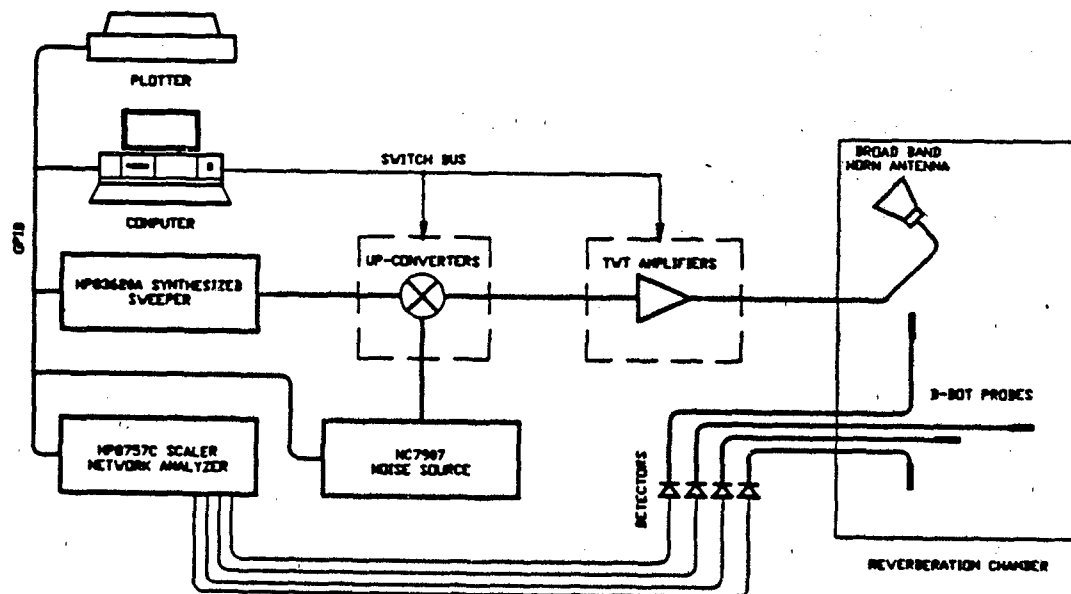


Figure 13. Experimental setup for swept tests on the NT enclosure.

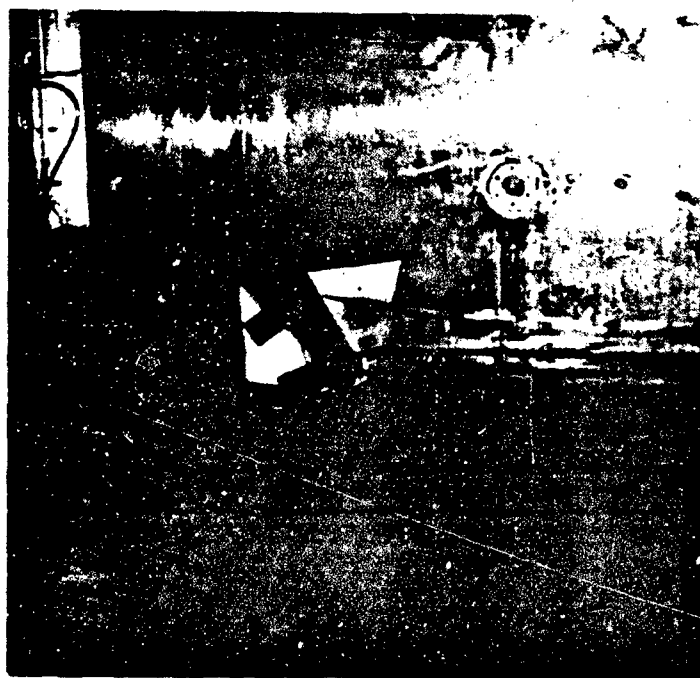


Figure 14. The NT enclosure: view of horn and probes.

PL-TR-91-1036

Output from the B-dot probes is converted to a signal measurable by the HP8757C Scaler Network Analyzer via one of four HP85025A AC/DC Detectors (0.01 to 18 Ghz, 23 dBm max). The HP8757C allows for a great deal of flexibility in making measurements of incoherent signals while maintaining a high degree of measurement accuracy. Simple data analysis such as detector ratios and averaging can be performed in near real time during the actual measurement by the scaler analyzer. The computer controller breaks the user supplied start and stop frequencies into individual bands that match the bands of the TWTs and up-converters, and then it instructs the HP8757C to acquire the appropriate data for each band while it provides the switching signals to the TWT and up-converter banks. The data from each band are then sampled in accordance with the user directed number of data points and a complete sweep is constructed.

FIELD UNIFORMITY SWEPT MEASUREMENTS (GIFT Box)

The GIFT Box is a 30 x 36 x 36 in welded aluminum enclosure with one large (27 in diameter) access hatch in the front and two other smaller (14.5 in diameter) access panels, one on the side and one on the back. In addition, as shown in Figure 2, there is one 4.5 in diameter feed-through panel on the front where the signals for the two B-dot probes were routed through. Figures 15 and 16 depict the test configuration used during the GIFT Box swept field uniformity tests. With the exception of the amplifiers and the number of probes, this test configuration is very similar to that used for the NT enclosure tests. The TWTs were not available at the time this test was conducted; instead, a set of high gain small signal amplifiers was used on the receiving side of the circuit to boost the B-dot output to levels well within the dynamic range of the Scaler Analyzer.

THE Q MEASUREMENTS (NT and GIFT Box)

The test configuration used to measure the Q of the NT enclosure is shown in Figure 17 (the GIFT box setup is similar except small signal amplifiers were used rather than TWTs). The significant difference between the two configurations is the same as in the case of the swept tests (TWT amplifiers versus small signal). Further, computer control of the sources, modulators, and amplifiers is similar to the swept case except that a single frequency is

selected for each measurement and the Synthesized Sweeper is placed in the pulse modulation mode. The HP3314A Function Generator is used to supply a TTL compatible square wave to the Synthesized Sweeper to chop the output of the sweeper at a relatively low frequency (10 to 100 KHz). The chopped signal is then supplied to the up-converter bank for modulation by the band limited WGN source. Both the horn input signal and the signal received by the B-dot probe are detected using HP423B Crystal Detectors and sent to the DSA 602 Digitizing Signal Analyzer for averaging and rise time measurements. It should be noted that because negative detectors are used, the B-dot signal rise time is equivalent to the relaxation time of the enclosure.

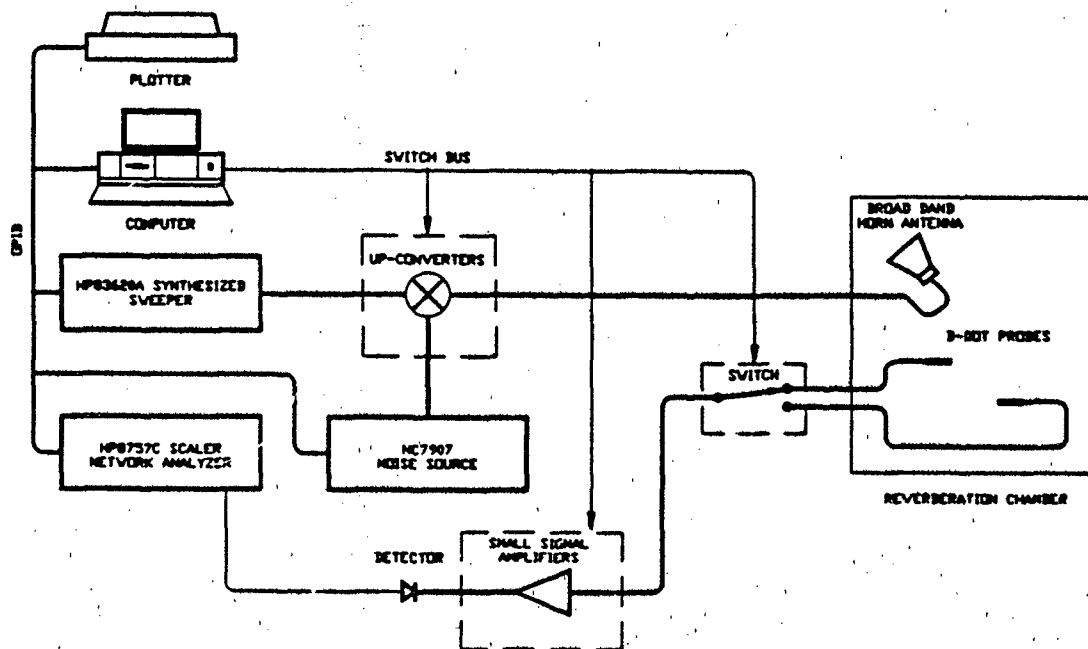


Figure 15. Experimental test setup for swept tests on the GIFT box enclosure.



Figure 16. The GIFT box enclosure: view of horn and probes.

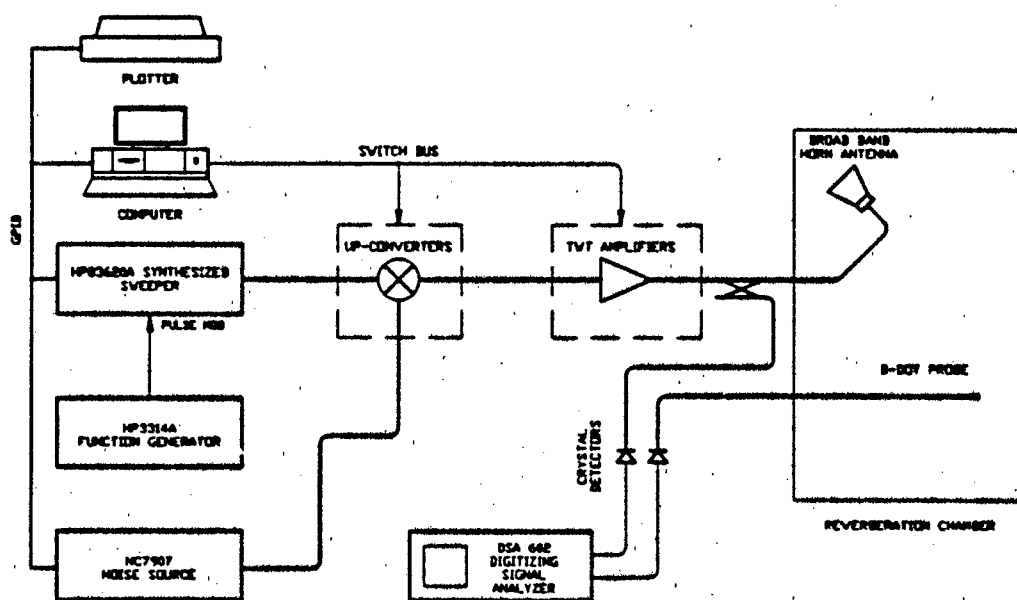


Figure 17. Test configuration used to measure Q of the NT enclosure.

TEST PROCEDURES

FIELD UNIFORMITY TESTS

Field uniformity tests were conducted on both the NT and GIFT Box enclosures to determine the effectiveness of the frequency stir method at reducing localized average field gradients. Using the test configurations described above, B-dot probes were used to measure the power ratios of the magnetic flux densities at randomly selected locations and vector orientations within the enclosures. Using Equation 3, for the monochromatic case (no modulation) and with the frequency fixed, the ratio of the power measured at the analyzer between any two probe locations, A and B, can be expressed as:

$$\frac{P_A}{P_B} = \frac{V_A^2 / (2Z)}{V_B^2 / (2Z)} = \left(\frac{B_{0A}}{B_{0B}} \right)^2 = \left(\frac{H_{0A}}{H_{0B}} \right)^2 \quad (56)$$

where

P_A/P_B - The power ratio of the probe outputs as directly measured by the analyzer.

V_A, V_B - The amplitude of the voltage produced by the B-dot probes.

Z - Impedance of the measuring device.

H_{0A}/H_{0B} - The ratio of the magnetic fields at locations A and B oriented along the axis of the probes.

When modulation is used the signal being measured by the analyzer is no longer monochromatic and therefore the power ratio analysis is slightly more complex. Using the probe's transfer function, Equation 2, the power measured by the analyzer will be:

$$P = \frac{1}{2\pi} \int_{\omega_c - BW/2}^{\omega_c + BW/2} |G(j\omega)|^2 S(\omega) d\omega \quad (57)$$

where

ω_c - Center frequency of the received signal.

BW - Bandwidth of the received signal.

$S(\omega)$ - Power Spectral density of the magnetic field at the probe location.

Therefore, the ratio of the power measured can be expressed as:

$$\frac{P_A}{P_B} = \frac{\int_{\omega_c - BW/2}^{\omega_c + BW/2} |G(j\omega)|^2 S_A(\omega) d\omega}{\int_{\omega_c - BW/2}^{\omega_c + BW/2} |G(j\omega)|^2 S_B(\omega) d\omega} \quad (58)$$

Clearly this equation can only represent the power ratio of the magnetic fields when the square of the magnitude of the transfer function G is constant over the interval $\omega_c - BW/2 < \omega < \omega_c + BW/2$. From Equation 2, the percent variation of G^2 can be easily written:

$$y = |G(j\omega)|^2 = A_o^2 \omega^2$$

$$Error = \frac{\Delta y}{y} = \frac{2 A_o^2 \omega BW}{A_o^2 \omega^2} = \frac{BW}{\pi f} \quad (59)$$

At the lowest frequency (1 GHz) and the widest agility bandwidth (100 MHz) used in this experiment, the variation is ≈ 3 percent. It is therefore evident that for any given frequency the field variation between two points can be determined directly from the test configuration discussed earlier. It is not, however, practical to fix the frequency and move the probes around the volume of the enclosures until the maximum field variations are found. Instead, the maximum and minimum field locations are forced to move within

the volume by sweeping the center frequency of the injected signal. As the center frequency is swept, new modal frequencies are encompassed in the signal's bandwidth while lower modal frequencies drop off. Thus the maxima and minima of the fields move around the enclosure passing by the probes as they move. The spatial variation of the fields can therefore be approximated by observing the maximum variations in the swept data provided a sufficiently large frequency interval is used.

Using the method described above, swept tests were conducted on the NT enclosure from 1 through 4 GHz with both monochromatic and up-converted noise with bandwidths of 10, 20, 50, and 100 MHz. Ratio measurements were taken directly using the HP85025A detectors as described in the test configuration above. The copper jacket 0.141 cable used between the probes and the feed-throughs at the bulkhead were cut to the same length and hence their insertion losses were measured to be within a few tenths of a decibel of each other and therefore ignored. The GIFT Box sweeps were conducted from 1 through 8 GHz. As with the NT enclosure, both monochromatic and up-converted noise with bandwidths of 10, 20, 50, and 100 MHz were used. However, because the small signal amplifiers were used on the receiving side of the circuit, separate sweeps for each probe were taken. The software was then used to convert the measurements to a ratio similar to that of the NT enclosure data.

THE Q MEASUREMENTS

The method used here to measure the Q of the two enclosures is a modification of the method developed by the Naval Surface Weapon Center. The 1/e decay time of the energy stored in the cavity can be expressed as [Ref. 12]:

$$\tau = \frac{Q}{2\pi f_0} \quad (60)$$

The Weapon Center measured the energy decay waveform produced by a pulsed RF input for many positions of the paddle wheel of a mode-stir chamber. Then by calculating the fall time of the ensemble average, they determined the composite Q from the above equation.

PL-TR-91-1036

Since there is no paddle wheel used in this technique, the Q of the cavities was measured slightly differently. Employing the frequency stir method and the test configuration described earlier, the relaxation time of the enclosures was determined by using the measured fall time of the ensemble average of the detected pulse train. This would seem to be a valid method to determine the fall time of the stored energy in the cavities because the ensemble defined by each pulse contains information from both the noise envelope and the energy decay waveform, but since the ensemble average of the noise envelope is a constant, the ensemble average of many of the pulses is proportional to the stored energy waveform. Therefore, the fall time of the ensemble average is equal to the fall time of the stored energy waveform.

RESULTS

SWEPT MEASUREMENTS

Figure 18 depicts the results of the swept measurements for the NT enclosure from 1 to 4 GHz. As indicated, agility bandwidths of 0, 10, 50, and 100 MHz are shown (the results of the 20 MHz agility bandwidth sweeps are not shown because of their similarity to the 10 MHz data) for the measured power ratio of probes C and D. These data are typical of the data taken for all combinations of the probe A, B, C, and D. The theoretical number of eigenmodes stimulated, predicted standard deviation, measured standard deviation, and ψ as defined by Equation 52 are given in Tables 2 and 3 for

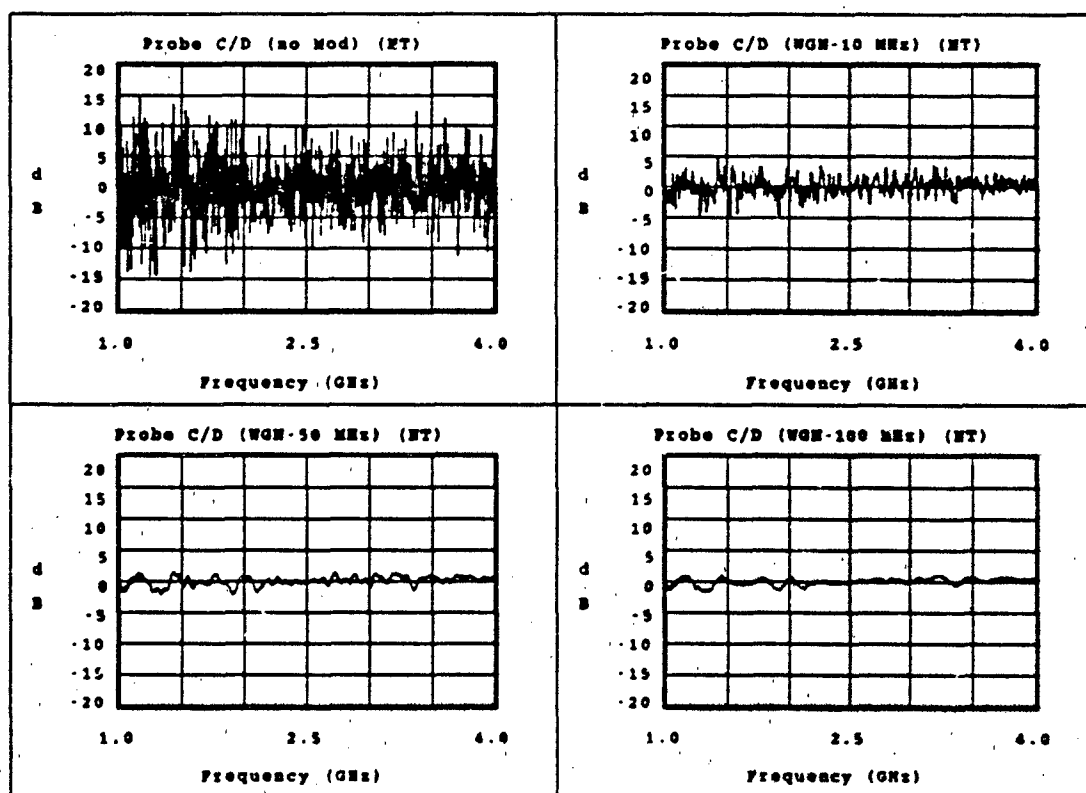


Figure 18. Measured power ratios of probes C and D for the NT enclosure with an agility bandwidth of 0, 10, 50 and 100 MHz.

Table 2. Homogeneity measurements for the NT enclosure.

Probe C/D

| Freq. (GHz) | Agility BW (MHz) | N | σ Predicted | σ Measured | ψ Measured |
|----------------|---------------------|------|-----------------------|----------------------|--------------------|
| 1.0-2.0 | 0 | - | - | 5.1 | 18.2 |
| | 10.0 | 32 | 1.7 | 1.7 | 5.1 |
| | 20.0 | 63 | 1.2 | 1.7 | 4.1 |
| | 50.0 | 158 | 0.76 | 0.92 | 2.1 |
| | 100.0 | 316 | 0.52 | 0.68 | 1.7 |
| 2.0-3.0 | 0 | - | - | 3.7 | 11.6 |
| | 10.0 | 126 | 0.86 | 1.3 | 3.5 |
| | 20.0 | 252 | 0.60 | 0.97 | 2.8 |
| | 50.0 | 630 | 0.38 | 0.58 | 1.8 |
| | 100.0 | 1262 | 0.27 | 0.37 | 1.3 |
| 3.0-4.0 | 0 | - | - | 3.7 | 14.0 |
| | 10.0 | 284 | 0.52 | 1.2 | 3.9 |
| | 20.0 | 568 | 0.39 | 0.84 | 2.8 |
| | 50.0 | 1420 | 0.26 | 0.54 | 1.5 |
| | 100.0 | 2824 | 0.19 | 0.34 | 1.1 |

Table 3. Homogeneity measurements for the GIFT box.

| Probe A/B | | | | | |
|----------------|---------------------|-----|-----------------------|----------------------|--------------------|
| Freq. (GHz) | Agility BW (MHz) | N | σ Predicted | σ Measured | ψ Measured |
| 1.0-2.0 | 0 | - | - | 7.9 | 26.3 |
| | 10.0 | 6 | 4.9 | 3.4 | 10.2 |
| | 20.0 | 12 | 3.0 | 2.8 | 8.1 |
| | 50.0 | 30 | 1.8 | 1.9 | 5.3 |
| | 100.0 | 59 | 1.3 | 1.4 | 2.8 |
| 2.0-3.0 | 0 | - | - | 5.5 | 20.0 |
| | 10.0 | 24 | 2.0 | 2.4 | 8.3 |
| | 20.0 | 47 | 1.4 | 1.8 | 6.3 |
| | 50.0 | 119 | 0.90 | 1.2 | 4.1 |
| | 100.0 | 237 | 0.60 | 1.0 | 3.6 |
| 3.0-4.0 | 0 | - | - | 5.2 | 19.1 |
| | 10.0 | 53 | 1.3 | 2.4 | 8.5 |
| | 20.0 | 107 | 0.92 | 1.8 | 4.9 |
| | 50.0 | 256 | 0.59 | 1.1 | 3.9 |
| | 100.0 | 534 | 0.40 | 0.89 | 2.6 |

1 GHz frequency ranges for each agility bandwidth. The Monte Carlo simulation predicts the standard deviation well for values >1 . It is believed that the setup's random and systematic errors begin to dominate the standard deviation measurements when the standard deviation begins to drop below 1. Therefore, data above 4 GHz are not shown for the GIFT box. The largest source of these errors is probably due to the systematic errors between the two probes used for the measurement. The particular probes used here have shown differences as large as a few decibels as the frequency and E-field orientation are varied.

As mentioned earlier, a normal distribution seems to be an adequate model for the density distribution of the ratio data. Figure 19 shows the typical results of fitting the ratio data (in decibel format) to a normal

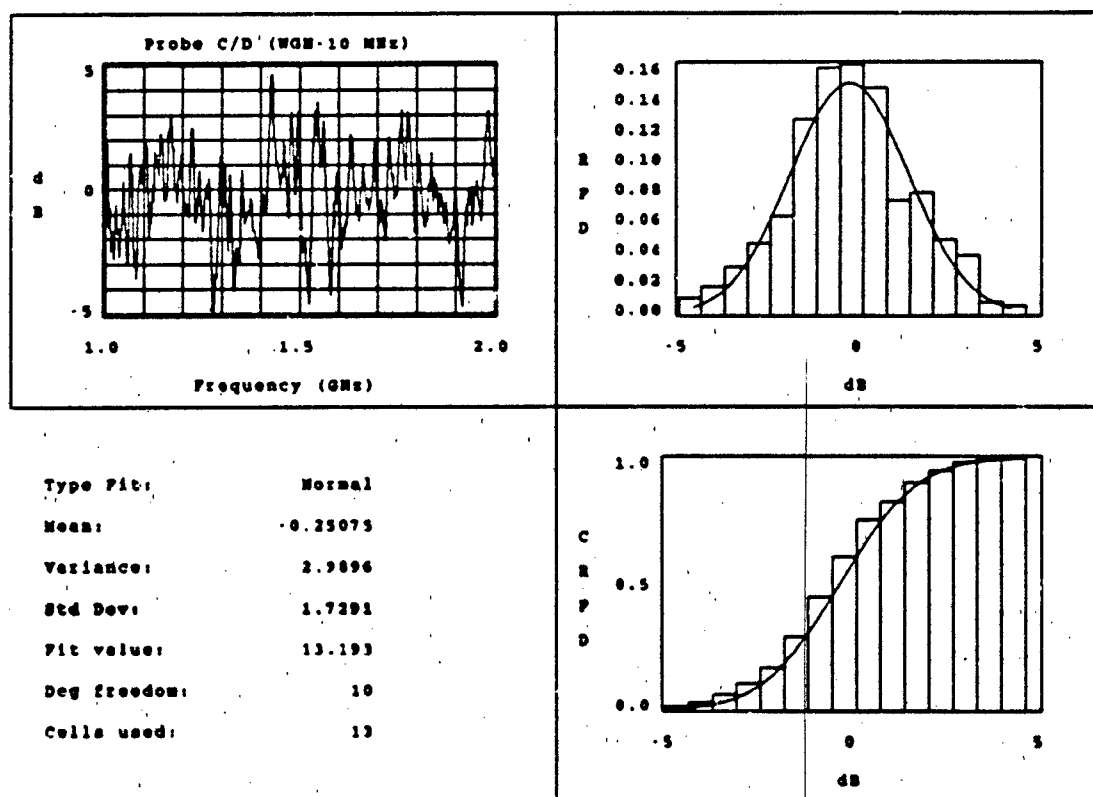


Figure 19. Goodness of fit test, NT enclosure, 10 MHz agility bandwidth, 1 to 2 GHz.

distribution. The histograms represent the relative frequency distributions (RFD) and the cumulative relative frequency distributions (CRFD) for the actual data. These RFDs are formed by dividing the abscissa of the data into equally sized cells and counting the number of points falling in each cell. The cell count is then divided by the total number of points. The CRDF is simply a running sum of the cell counts. The continuous plots are the RFD and CRDF of the theoretical model being fitted.

The goodness of fit test used is the Person's chi-square statistic [Ref. '9]. The smaller the fit value, the better the fit. In fact, by looking up the fit value in a table of chi-square distributions of n degrees of freedom, the probability that discrepancies of this order (the fit value) or larger would be seen, given the model is correct, can be found. In all cases, the distribution of the ratio data (in decibels) proved to have acceptable normal distribution fits.

2 MEASUREMENTS

Figure 20 shows the quality factor of both enclosures as measured using the technique described earlier. No attempt is made at predicting the Q based on the earlier theoretical Q discussions because the wall conductivity is difficult to assess for these enclosures. They both are in very poor condition and have accumulated scale on their interiors.

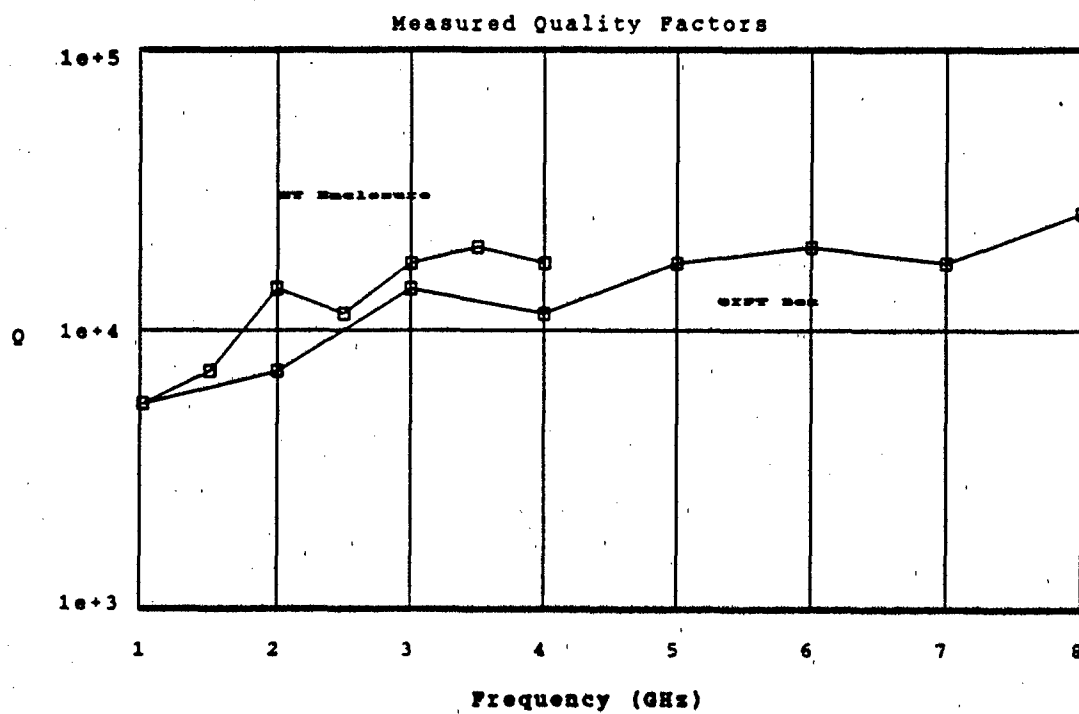


Figure 20. Measured Q for both enclosures.

CONCLUSION

From the data gathered to date, it would seem that the frequency stir technique has potential application in electromagnetic interference and susceptibility testing. For practically-sized chambers, field uniformities equivalent to the paddle wheel mode-stir technique can easily be achieved with relatively narrow agility bandwidths (5 MHz) while test time is dramatically improved. Another potential application of the frequency stir technique is to directly pump a large test article with the up-converted noise so that its own cavities become the mode-stir chamber. This may be helpful in both upset testing for assets too large to fit in a chamber and sniff testing (finding the leaky apertures by using a probe to sniff around the exterior of the test article). Lastly, because of the inherent smoothing of the coupling data that takes place when using this technique, it may have application in plane wave illumination in an anechoic chamber to acquire coupling trend data directly or reduce the dynamic range required by the measuring instruments.

It has also been demonstrated that when predicting the Q of a reverberation chamber, the effect of the measuring, and in some cases the transmitting antenna, must be considered. They, in effect, act as apertures in the chamber that vary their size with frequency. The largest potential effect exists at the low end of the frequency spectrum where the effective area of the antenna is very large and can in fact dominate the net Q of the cavity. It is therefore better to use probes or antennae which have relatively small effective areas such as B-dot or D-dot probes.

REFERENCES

1. Crawford, M.L. and Koepke, G.H., Design, Evaluation, and Use of a Reverberation Chamber for Performing Electromagnetic Susceptibility/Vulnerability Measurements, National Bureau of Standards (U.S.) NBS Tech. Note 1092, April 1986.
2. Pozar, D.M., Microwave Engineering, Addison-Wesley Publishing Co., Reading, MA, 1990.
3. Price, R.H., et al, Determination of the Statistical Distribution of Electromagnetic Field Amplitudes in Complex Cavities, Harry Diamond Laboratory, Adelphia, MD, June 1988.
4. Liu, B.H.; Chang, D.C.; and Ma, M.T., Eigenmodes and the Composite Quality Factor of a Reverberating Chamber, National Bureau of Standards (U.S.) NBS Tech. Note 1066, August 1983.
5. Carlson, A.B., Communication Systems: An Introduction to Signals and Noise in Electrical Communication, McGraw-Hill, New York, NY, 1975.
6. White, R.J. and Mardiguian, M., Electromagnetic Shielding. A Handbook Series on Electromagnetic Interference, Don White Consultants, Germantown, MD, 1974.
7. Crawford, M.L.; Ma, T. M.; Ladbury, J. M.; and Riddle, B. F., Measurement and Evaluation of a TEM/Reverberating Chamber, Nat. Inst. of Stand. NIST Tech. Note 1342; 1990 July.
8. Tai, C.T., "On the Definition of the Effective Aperture of Antennas," IEEE Trans. on Antennas and Propagation, AP-9: 224-225, March 1961.
9. Rice, J.A., Mathematical Statistics and Data Analysis, Wadsworth Inc., Belmont, CA, 1988.
10. Walpole, R.W. and Myers, R.H., Probability and Statistics for Engineers and Scientists, MacMillan Publishing Co., New York, NY, 1978.
11. Department of Defense Methodology Guidelines for High Power Microwave (HPM) Susceptibility Assessments, Office of the Secretary of Defense, Washington, DC, January 1990.
12. Richardson, R.E., "Mode Stirred Chamber Calibration Factor and Relaxation Time," IEEE Trans. on Instrumentation and Measurements, Vol. IM-34 #4, pp 190-193, December 1985.

**END
FILMED**

DATE:

1-92

DTIC